

Bivariate Luminosity Function of Galaxy Pairs

SHUAI FENG (冯帅),^{1,2} SHI-YIN SHEN (沈世银),^{1,3} FANG-TING YUAN (袁方婷),¹ A-LI LUO (罗阿里),⁴
JIAN-NAN ZHANG (张健楠),⁴ MENG-XIN WANG (汪梦欣),⁴ XIA WANG (汪霞),⁴ YIN-BI LI (李荫碧),⁴ WEN HOU (侯文),⁴
XIAO KONG (孔啸),⁴ YAN-XIN GUO (郭炎鑫),⁴ AND FANG ZUO (左芳)⁴

¹Key Laboratory for Research in Galaxies and Cosmology, Shanghai Astronomical Observatory, Chinese Academy of Sciences,
80 Nandan Road, Shanghai 200030, China

²University of the Chinese Academy of Sciences, No.19A Yuquan Road, Beijing 100049, China

³Key Lab for Astrophysics, Shanghai 200234, China

⁴Key Laboratory of Optical Astronomy, National Astronomical Observatories, Chinese Academy of Sciences, Beijing 100101, China

ABSTRACT

We measure the bivariate luminosity function (BLF) of galaxy pairs and use it to probe and characterize the galaxy-galaxy interaction between pair members. The galaxy pair sample is selected from the main galaxy sample of Sloan Digital Sky Survey and supplied with a significant number of redshifts from the LAMOST spectral and GAMA surveys. We find the BLFs depend on the projected distance d_p between pair members. At large separation $d_p > 150 h^{-1}$ kpc, the BLF degenerates into a luminosity function (LF) of single galaxies, indicating few interactions between pair members. At $100 h^{-1}$ kpc $\leq d_p \leq 150 h^{-1}$ kpc, the BLF starts to show the correlation between pair members, in the sense that the shape of the conditional luminosity function (CLF) of one member galaxy starts to depend on the luminosity of the other member galaxy. Specifically, the CLF with a brighter companion has a steeper faint-end slope, which becomes even more significant at $50 h^{-1}$ kpc $\leq d_p \leq 100 h^{-1}$ kpc. This behavior is consistent with the scenario, *and also is the observational evidence*, that dynamic friction drives massive major merger pairs to merge more quickly. At close distance $d_p \leq 50 h^{-1}$ kpc, besides the merging time-scale effect, the BLF also shows an overall brightening of $\Delta M_r \geq 0.04$ mag, which reveals the enhanced star formation of the close-pair phase. By combining another statistical conclusion that the star formation rate of late-type galaxies in close pairs is enhanced at a level of about 40%, we further conclude that the average starburst time-scale of close pairs is as long as 0.4 Gyr.

Keywords: galaxies: interaction – galaxies: luminosity function, mass function

1. INTRODUCTION

In a hierarchical galaxy formation diagram, the galaxy-galaxy interaction plays a key role in shaping the galaxy evolution path. As the simplest galaxy ‘systems’, galaxy pairs are the ideal places to study the interactions between galaxies. Recent decades have proven that the interaction in close pairs (e.g., $d_p \leq 50 h^{-1}$ kpc) could change the physical properties of galaxies significantly. Compared to field galaxies, the galaxies with close encounters typically have disturbed morphologies (Toomre & Toomre 1972; Hernández-Toledo et al. 2005, 2006; Patton et al. 2016), enhanced star formation rates

(Barton et al. 2000; Woods et al. 2006; Ellison et al. 2008; Scudder et al. 2012; Davies et al. 2015), diluted nuclear metallicities (Ellison et al. 2008; Kewley et al. 2010; Scudder et al. 2012), and overabundances of active galactic nuclei (Ellison et al. 2008, 2011; Liu et al. 2011; Fu et al. 2018). On the other hand, it is far from clear how the interaction in wide pairs (e.g., $d_p \geq 50 h^{-1}$ kpc) influences galaxy evolution. Those wide pairs do not show significant differences from the field galaxies, such as morphological asymmetry and enhanced star formation rate (Patton et al. 2013; Patton et al. 2016).

Besides changing their physical properties, galaxy-galaxy interaction also shapes galaxy evolution through galaxy merging. In galaxy pairs, the orbital energy and angular momentum of pair members gradually dissipate through dynamic friction and then finally merge.

Numerical simulations show, that the typical merging time-scale is about 1 – 2 Gyr and mainly depends on the masses of both pair members (Lacey & Cole 1994; Boylan-Kolchin et al. 2008; Jiang et al. 2008; Lotz et al. 2010a). As a result, the relative number density of galaxy pairs would deviate from a random combination of field galaxies, even when the changes in their physical properties seem negligible.

In general, in the galaxy pair environment, the enhanced star formation induced by close interaction (e.g., tidal effect) will brighten the galaxies. On the other hand, if the merging time-scale of more massive galaxies is shorter (e.g., Jiang et al. 2014), there would be a lower fraction of bright galaxies in pairs than that in the field. Therefore, the luminosity function of galaxies in pairs would be different from that of field galaxies. Apart from the general difference, the interaction between pair members further complicates the statistical properties of the galaxies in pairs. For example, the galaxies in major merger pairs (those with mass ratio larger than 1:3) are believed to suffer stronger interaction (therefore more enhanced star formation) than in minor ones (e.g., Davies et al. 2015). Also, the merging time-scale is shown to be strongly dependent on the mass ratio of pair members (e.g., Boylan-Kolchin et al. 2008). Therefore, as a result of these complex interactions, the physical and statistical properties of pair members would not only deviate from those of single galaxies but would also be strongly coupled to each other.

The luminosity function (LF), as a basic statistical description of the relative number of galaxies with different luminosity, provides a fundamental constraint on the modeling of galaxy formation and evolution. For galaxy pairs, there are two different types of LFs, the univariate LF (ULF) and bivariate LF (BLF). The ULF does not distinguish the pair members and provides a measurement of the pair fraction of galaxies (Xu & Sulentic 1991; Xu et al. 2004; Domingue et al. 2009). For example, Domingue et al. (2009) found that the ULF of galaxy pairs in K_S band is very similar to the global LF of the galaxy sample, which implies a constant pair fraction of $\sim 1.6\%$. Comparing with ULF, BLF contains more information, in particular, on the correlations of variables (Sodre & Lahav 1993; Ball et al. 2006; Takeuchi et al. 2013). Robotham et al. (2014) investigated the fraction of galaxy pairs with different mass configurations using a bivariate measurement of stellar mass distribution of pair members. However, the internal correlation between pair members has not been addressed.

To have a comprehensive description of galaxy pairs, where both the configuration of galaxy pairs (e.g., merg-

ing time-scale) and the physical properties of pair members (e.g., enhanced star formation) is taken into account, the BLF of pair members $\Phi(M_A, M_B)$ might be an ideal diagnostic tool. If we assume that the galaxy pairs are initially built from random pairing of single galaxies, we would expect that the initial BLF of galaxy pairs could degenerate into the LF of single galaxies, in the sense that the shape of the conditional luminosity function (CLF) of one member galaxy $\Phi(M_A|M_B)$ would not depend on its companion luminosity M_B . Therefore, this assumption could be used to test the critical distance where the galaxy-galaxy interaction starts. As the galaxy pairs evolve, the physical interactions change the luminosities of pair members, whereas the merging process further alters their relative number densities. Both mechanisms will change and shape the BLF of galaxy pairs.

To have an accurate measurement of $\Phi(M_A, M_B)$, a large and well-defined galaxy pair sample is required. The largest galaxy pair sample at low redshift to date is built based on the main galaxy sample of the Sloan Digital Sky Survey (SDSS, York et al. 2000), e.g., Ellison et al. (2008). In this study, we will also build the galaxy pair sample based on SDSS galaxies. Compared with the previous works, we have two main improvements. First, we have supplied a large number of redshifts from the LAMOST spectral survey (Shen et al. 2016), which increases both the total number and completeness of the galaxy pair sample (Section 2). Second, we extend the projected distance threshold out to $200 h^{-1}$ kpc during galaxy pair selection. This threshold is more extended than most of the other studies ($\sim 100 h^{-1}$ kpc, e.g., Scudder et al. 2012), where the galaxy-galaxy interaction effects are only found at smaller separation.

This paper is organized as follows. In Section 2 we introduce the galaxy sample, criteria of galaxy pair selection and incompleteness correction. Then, we measure and parameterize the BLFs of galaxy pairs as a function of projection distance in Section 3. In Section 4, we build toy models to discuss the physical implications of the BLFs. Finally, we give a summary in Section 5. Throughout this paper, we assume standard Λ -CDM concordance cosmology with $\Omega_m = 0.3$, $\Omega_\Lambda = 0.7$ and $h = H_0 / 100 \text{ km s}^{-1} \text{ Mpc}^{-1}$.

Throughout this paper, we use L_A and L_B to denote luminosities of pair members, where A and B are assigned to the pair members randomly. On the other hand, when we consider luminosities of the primary and secondary galaxies, we use L_1 and L_2 instead. We denote the mass of pair members in a similar way.

2. DATA

In this section, we describe the parent galaxy sample, the selection algorithm for galaxy pairs and the correction for spectroscopic incompleteness.

2.1. Parent Sample

The parent galaxy catalog we use is the New York University Value-Added Galaxy Catalog (NYU-VAGC; Blanton et al. 2005) of the SDSS DR7 (Abazajian et al. 2009), which is a cross-matched collection of galaxy catalogs including extra redshifts from other surveys (e.g., 2dF, PSCz, RC3). To have high redshift completeness, following the main galaxy sample (MGS, Strauss et al. 2002) of SDSS, we take the galaxies with Galactic extinction corrected magnitude in the range of $14.0 \leq m_r \leq 17.77$. In NYU-VAGC, the number of galaxies in this magnitude range is 746,950. We refer to these galaxies as the parent photometric sample. Among them, 696,245 have redshifts, which is contributed by different surveys, but mainly from the SDSS DR7 (686,398, > 98.6%). The small fraction of galaxies without redshifts in the SDSS MGS is primarily caused by the fiber collision effect (Shen et al. 2016).

The MGS galaxies without redshifts in the SDSS DR7 were continually targeted in the SDSS III and IV with spare fibers. We matched the parent photometric sample with the latest SDSS data release, DR14 (Abolfathi et al. 2018)¹ and obtained 8,532 extra redshifts. Moreover, these MGS galaxies without redshifts in the SDSS DR7 have also been compiled as a complementary galaxy sample and targeted in the LAMOST spectral survey (Cui et al. 2012; Zhao et al. 2012; Luo et al. 2015). In the LAMOST data release 5, we find an additional 7,004 galaxies with spectroscopic redshifts. We also matched the parent photometric sample with data release 2 of the GAMA survey (Liske et al. 2015) and obtained a further 1,024 redshifts. For a few galaxies having more than one redshifts measured by different surveys, we set the priority as follows: SDSS > LAMOST DR5 > GAMA DR2 > others in NYU-VAGC. Finally, we obtained redshifts for 711,347 galaxies in total, which results in spectroscopic completeness of 95.2%. The exact numbers of redshifts obtained from different surveys are listed in Table 1.

2.2. Pair Selection

We use a friend-of-friend (FOF) algorithm to select galaxy pairs from the parent sample. The main selection criteria are listed as follows:

Table 1. Redshifts of the parent sample.

| Redshift Catalog | Redshift Number |
|-----------------------------|-----------------|
| SDSS DR14 | 694,930 |
| LAMOST DR5 | 7,004 |
| GAMA DR2 | 1,024 |
| Others from NYU-VAGC | 8,339 |
| Spectroscopic Sample in MGS | 711,347 |
| Photometric Sample in MGS | 746,950 |

1. The line-of-sight velocity difference of two galaxies satisfies $|\Delta v| \leq 500 \text{ km s}^{-1}$.
2. The projected distance between two galaxies is in the range of $10 h^{-1} \text{ kpc} \leq d_p \leq 200 h^{-1} \text{ kpc}$.
3. Each galaxy has only one neighbor satisfying the above criteria.

We exclude the very close galaxy pairs ($d_p < 10 h^{-1} \text{ kpc}$) to avoid the very peculiar morphology and unreliable deblending photometry. We require that each galaxy only has one neighbor to avoid those galaxies in a compact group environment. Since our galaxy sample is still not 100 % complete in spectroscopy, there are 9,175 galaxy pairs having neighbors within $10 h^{-1} \text{ kpc} \leq d_p \leq 200 h^{-1} \text{ kpc}$, and these neighbors do not have redshifts. In this case, some of the pairs would violate the ‘isolated’ criteria if their neighbors also have the same redshifts as them. For the sake of safety, we have not considered these galaxy pairs in the BLF calculation. Finally, we have 46,510 galaxy pairs.

We also have cross-matched the galaxy pair sample with the SDSS group catalog of Yang et al. (2007). We find that less than one fifth (9,188/46,510) of them are located in the groups with more than two members. For these galaxy pairs in *groups*, since the other members are located much further away $d_p > 200 h^{-1} \text{ kpc}$, the influences of external interaction from other members at such distances is negligible (see Section 3.2). We also have tested that the exclusion of these pairs in *groups* would not change any of our conclusions except to increase the uncertainty.

In Figure 1, we show the distributions of some basic parameters of the galaxy pair sample, including the *r*-band magnitudes and redshifts of pair members, the projected distances and velocity differences of galaxy pairs. In each of the top two panels, the global distribution of the parent galaxy sample is overlaid as a dashed histogram for comparison. The galaxies in pairs show significant differences from the parent galaxy sample. These differences are mainly caused by the fiber collision effect, where the more distant (fainter) pairs are

¹ There are no new extra redshifts in the SDSS DR15.

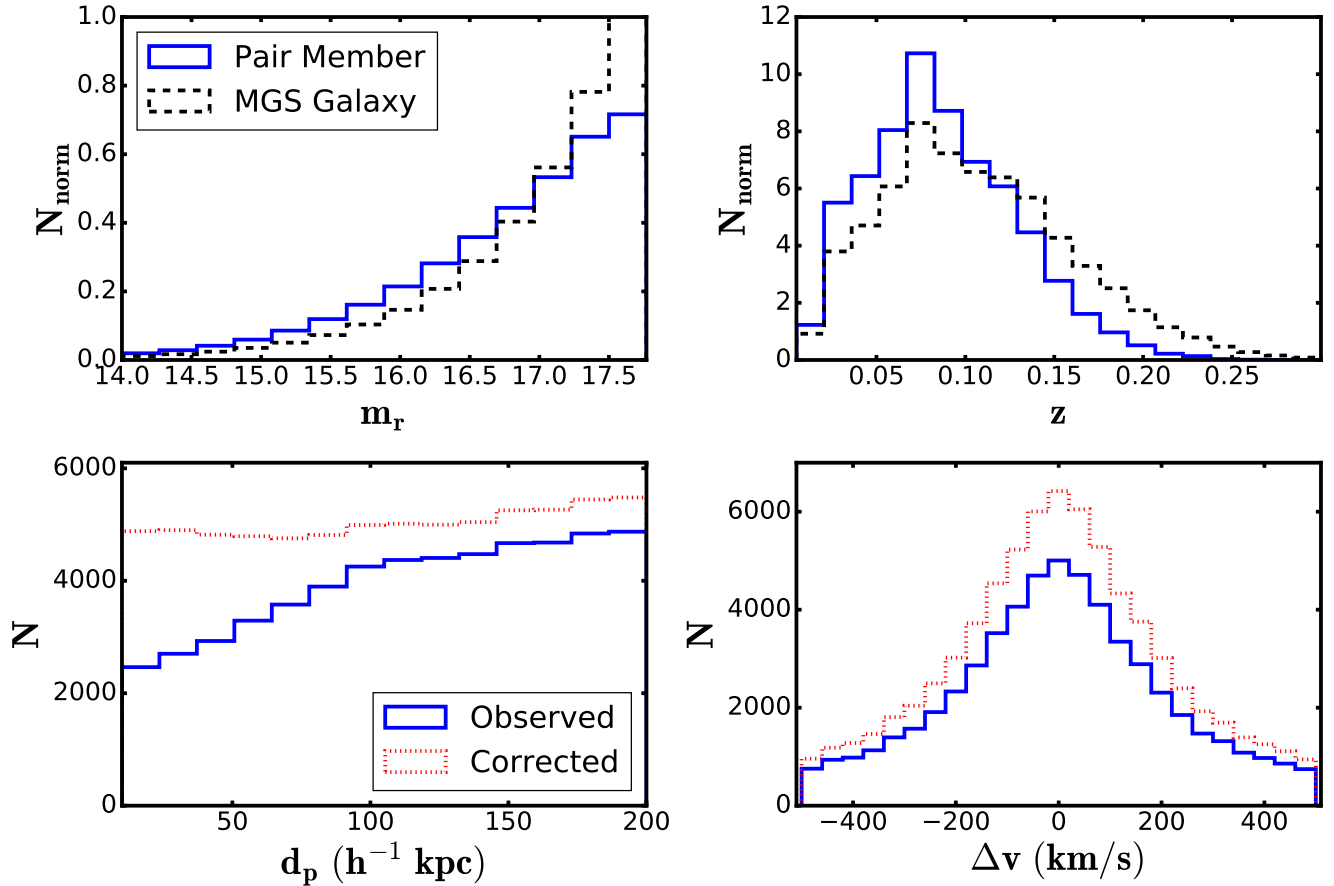


Figure 1. *Top:* the apparent magnitude and redshift distributions of the pair members (blue solid lines) and parent sample (black dashed lines). *Bottom:* the projected distance and velocity difference distributions of the galaxy pair sample (blue solid lines), where the red dotted lines show the corresponding distributions after spectroscopic incompleteness correction.

more likely to be missed because of their closer angular separation. In the bottom two panels, we show d_p and ΔV distribution of the galaxy pair sample with solid blue lines. As comparison, we also show the d_p and ΔV distribution of galaxy pairs after spectroscopic completeness correction (see Section 2.3) as red dotted lines. After correction of the incompleteness, the d_p distribution shows a quite flat distribution while the ΔV distribution is almost unchanged.

2.3. Spectroscopic Incompleteness

Although the completeness of the parent galaxy sample has been improved by supplementing lots of additional redshifts (Table 1), spectroscopic incompleteness still remains, especially for very close pairs. To demonstrate this effect, we show the distribution of the galaxy pair sample in $d_p - z$ plane (left panel of Figure 2). The red line in Figure 2 shows the $d_p - z$ relation for the angular separation of $\theta = 55''$, which is the minimum angular separation between any two SDSS fibers (York et al. 2000). The incompleteness at $\theta < 55''$ is still obvious.

To make corrections for the incompleteness of the galaxy pair sample, we calculate the spectroscopic completeness of the galaxy pairs with different angular separation as follows. We explore a series of annuli ($\theta \pm \Delta\theta/2$) around each galaxy of the parent galaxy sample. We set $\Delta\theta$ to be $3''$ and θ to span from $10''$ to $500''$, which corresponds to physical separations of $4 h^{-1}$ kpc and $200 h^{-1}$ kpc at redshift 0.03 respectively. For given θ , we first count the number of galaxies enclosed by all annuli as $N_{pp}(\theta)$, which is equivalent to the number of close-projected galaxies. Among them, we further count the number of its subsample as $N_{ss}(\theta)$, in which both two close-projected galaxies have spectroscopic redshifts, regardless of whether they are real galaxy pairs. Then, the spectroscopic completeness of our galaxy pair sample for the angular separation of θ can be expressed as

$$C_{\text{pair}}(\theta) = \frac{N_{ss}(\theta)}{N_{pp}(\theta)} \quad (1)$$

We show $C_{\text{pair}}(\theta)$ as the dots in the right panel of Figure 2, where the error bars show the uncertainties

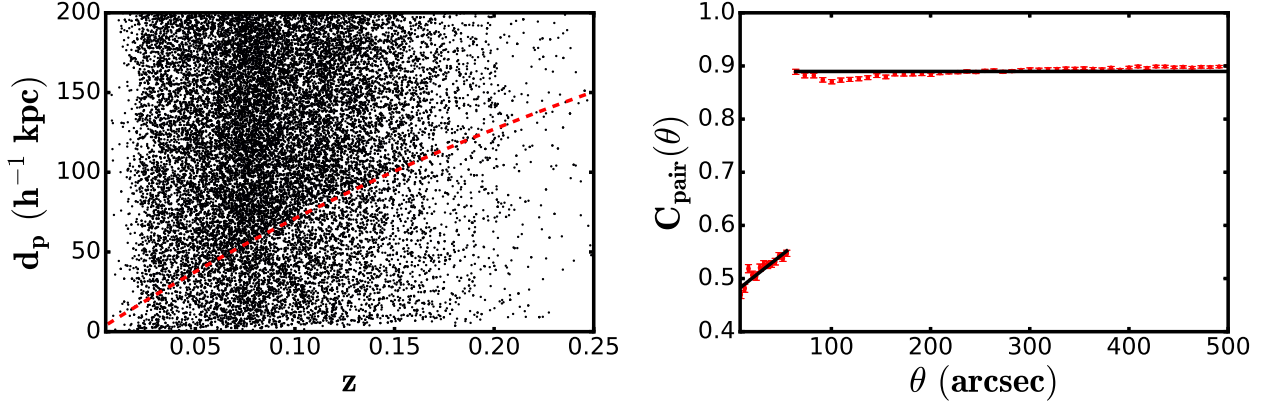


Figure 2. *Left panel:* the distribution of the galaxy pair sample in the $d_p - z$ plane, in which the red dashed line represents $\theta = 55''$. *Right panel:* the spectroscopic completeness as a function of angular separation θ . The black solid line shows the fitting formula of Equation 2. The error bars show the uncertainties of 68% confidence from Poisson statistics.

from Poisson statistics. As can be seen, the change of $C_{\text{pair}}(\theta)$ at $\theta = 55''$ is dramatic. At large separation $\theta > 55''$, $C_{\text{pair}}(\theta)$ is approximately a constant ~ 0.89 , which is roughly equal to the square of the global spectroscopic completeness of our parent sample (95.2%). At $\theta < 55''$, $C_{\text{pair}}(\theta)$ on average is about 50%, and systematically decreases with decreasing θ . Although the completeness of our galaxy pair sample is still far from 100%, it is much better than in previous studies ($\sim 30\%$, e.g. Ellison et al. 2008) where only SDSS DR7 data are available. Since most of our galaxy pairs have $\theta > 55''$, the average spectroscopic completeness of the galaxy pair sample reaches 82%.

For convenience, we fit $C_{\text{pair}}(\theta)$ with a step function,

$$C_{\text{pair}}(\theta) = \begin{cases} 0.889 & \theta \geq 55'' \\ 0.0015\theta + 0.471 & \theta < 55'' \end{cases} \quad (2)$$

which is also shown as the solid line in the right panel of Figure 2.

Besides the average completeness function shown by Equation 2, it should be emphasized that the completeness function of our galaxy pair sample varies over the sky. For example, the completeness in the sky coverage of the GAMA survey ($\sim 290 \text{ deg}^2$) is much higher than other areas since the GAMA has the completeness of $> 98\%$ down to $r < 17.77$ (Baldry et al. 2010). However, considering the extensive sky coverage of our galaxy pair sample ($\sim 7000 \text{ deg}^2$), we do not expect any cosmic variance effect would alter the statistical conclusions of this study.

3. BIVARIATE LUMINOSITY FUNCTION

In this section, we first introduce the algorithm of the BLF calculation and then present the BLF dependence on the projected distance of pair members. Next, we introduce an analytical formula to parametrize the shape

of the measured BLFs. At the end of this section, we discuss the ULF and the number density of galaxy pairs.

To build the LF, we calculate the $K + E$ corrected absolute magnitude of each galaxy at $z = 0.1$ following Blanton et al. (2003a),

$$M_r^{0.1} = m_r - 5 \log(d_L/10\text{pc}) - K_r^{0.1}(z) + (z - 0.1)Q$$

where m_r is the r -band apparent magnitude corrected for Galactic extinction, d_L is the luminosity distance, $K_r(z)$ is K-correction value calculated using the KCORRECT algorithm of Blanton & Roweis (2007), and Q is the evolution correction which equals to 1.62 for r -band (Blanton et al. 2003a).

3.1. Method

We take the extension of the non-parametric step-wise maximum likelihood estimator (SWML, Efsthathiou et al. 1988) for BLF calculation (Sodre & Lahav 1993). In this method, the BLF of galaxy pairs $\Phi(A, B)$ is defined as a step function,

$$\Phi(A, B) = \phi_{jk} \quad (j = 1, \dots, N_A; k = 1, \dots, N_B) \quad (3)$$

When the magnitudes of pair members A and B locate in absolute magnitude bin $A_j^- < A < A_k^+$ and $B_k^- < B < B_k^+$ respectively, the value of pair BLF equals to ϕ_{jk} . N_A and N_B are the magnitude bin numbers, and magnitude bin edges are set as

$$\begin{aligned} A_j^\pm &= A_j \pm \Delta A/2, \\ B_k^\pm &= B_k \pm \Delta B/2, \end{aligned}$$

where ΔA and ΔB are the bin widths.

Considering a magnitude-limited sample containing N_p galaxy pairs with the member absolute magnitudes (A_i, B_i), angular separation θ_i and redshift z_i respectively ($i = 1, \dots, N_p$), for given $\Phi(A, B)$, the probability

of observing i th galaxy pair is

$$p_i = \frac{\Phi(A_i, B_i)C_{\text{pair}}(\theta_i)}{\int_{A_{\text{faint}}(z_i)}^{A_{\text{bright}}(z_i)} \int_{B_{\text{faint}}(z_i)}^{B_{\text{bright}}(z_i)} \Phi(A, B)C_{\text{pair}}(\theta)dAdB}, \quad (4)$$

where $A_{\text{bright}}(z_i)$ and $A_{\text{faint}}(z_i)$ ($B_{\text{bright}}(z_i)$ and $B_{\text{faint}}(z_i)$) are the brightest and faintest absolute magnitude that the member of i th galaxy pair can be observed for the given apparent magnitude limit m_{bright} and m_{faint} . For our galaxy pair sample, the magnitude limits are $m_{\text{bright}} = 14.00$, $m_{\text{faint}} = 17.77$. Then the global likelihood \mathcal{L} is defined as the products of p_i for all pairs,

$$\mathcal{L} = \prod_{i=1}^{N_p} p_i. \quad (5)$$

To be specific, \mathcal{L} can be rewritten as follows,

$$\begin{aligned} \ln \mathcal{L} = & \sum_{i=1}^{N_p} \sum_{j=1}^{N_A} \sum_{k=1}^{N_B} W_{ijk} \ln[\phi_{jk} C_{\text{pair}}(\theta_i)] \\ & - \sum_{i=1}^{N_p} \ln \left(\sum_{j=1}^{N_A} \sum_{k=1}^{N_B} H_{ijk} \phi_{jk} \right) + \text{constant}. \end{aligned} \quad (6)$$

Here, we have defined two window functions,

$$W_{ijk} = \begin{cases} 1 & \text{if } -\Delta A/2 \leq A_i - A_j < \Delta A/2 \\ & \text{and } -\Delta B/2 \leq B_i - B_k < \Delta B/2 \\ 0 & \text{otherwise} \end{cases} \quad (7)$$

and

$$H_{ijk} = \frac{1}{\Delta A \Delta B} \int_{A^-}^{A'} \int_{B^-}^{B'} C_{\text{pair}}(\theta_i) dAdB \quad (8)$$

where

$$\begin{aligned} A' &= \max[A^-, \min(A^+, A_{\text{faint}}^i)], \\ B' &= \max[B^-, \min(B^+, B_{\text{faint}}^i)]. \end{aligned}$$

The maximum value of \mathcal{L} is calculated by solving $\partial \mathcal{L} / \partial \phi_{jk} = 0$. In practice, ϕ_{jk} is obtained through iteration:

$$\phi_{jk} = \frac{\sum_i^{N_p} W_{ijk}}{\sum_i^{N_p} (H_{ijk} / \sum_l^{N_A} \sum_m^{N_B} \phi_{lm} H_{ilm})}. \quad (9)$$

In the above calculation, the galaxies in pairs are assigned as member A and B randomly. The final BLF value of each bin is taken as the average of the corresponding diagonal bin. In this case, the final BLF satisfies $\Phi(A, B) = \Phi(B, A)$.

Similar to SWML, this method only provides the shape of BLF. The normalized density of the pair BLFs need to be estimated independently. For our galaxy pair

sample, the number density of the galaxy pairs is estimated by

$$n_{\text{pair}} = \sum_i^{N_p} \frac{1}{C_{\text{pair}}(\theta_i) V_{i,\text{max}}}, \quad (10)$$

where $V_{i,\text{max}}$ is the largest volume where i th galaxy pair is observable. Meanwhile, from the definition of BLF, the number density of galaxy pairs could also be expressed as

$$n_{\text{pair}} = \int_{A_{\text{min}}}^{A_{\text{max}}} \int_{B_{\text{min}}}^{B_{\text{max}}} \Phi(A, B) dAdB. \quad (11)$$

With the above two equations, the normalization parameter of BLF could finally be estimated.

The error of BLF is derived using the bootstrap algorithm. We make 100 bootstrap galaxy pair samples, and use the standard deviation of the best estimations of these 100 samples as the uncertainty of the BLF.

3.2. BLF Dependence on Projected Distance

We divide the galaxy pair sample into four subsamples according to the projected distances d_p between pair members and calculate the BLF of each subsample. The intervals of d_p are $10 \ h^{-1} \text{ kpc} \leq d_p \leq 50 \ h^{-1} \text{ kpc}$, $50 \ h^{-1} \text{ kpc} \leq d_p \leq 100 \ h^{-1} \text{ kpc}$, $100 \ h^{-1} \text{ kpc} \leq d_p \leq 150 \ h^{-1} \text{ kpc}$ and $150 \ h^{-1} \text{ kpc} \leq d_p \leq 200 \ h^{-1} \text{ kpc}$ respectively. The BLFs are only calculated in the magnitude range of $-22.5 \leq M_r \leq -18.0$, where the number of galaxy pairs is large enough to make high confidence statistics. The resulting BLFs are shown in Figure 3, where four rows represent four subsamples. In each row, the left and middle panels show the BLF value and relative error respectively. To interpret the BLF more understandably, we show two CLFs $\Phi(M_A | M_B = -21.25)$ and $\Phi(M_A | M_B = -19.25)$ extracted from both the BLF map and its error map. The right panels show that when the projected distance increases to $d_p \geq 150 \ h^{-1} \text{ kpc}$, $\Phi(M_A | M_B = -21.25)$ becomes indistinguishable from $\Phi(M_A | M_B = -19.25)$, indicating independence of two pair members. On the other hand, at $d_p \leq 150 \ h^{-1} \text{ kpc}$, the CLFs start to show a discrepancy, and this discrepancy becomes even larger at smaller d_p .

The above BLF results explicitly show that the galaxies in pairs start to show interactions at a distance as far as $d_p \sim 150 \ h^{-1} \text{ kpc}$. Except for a slight SFR enhancement out to $d_p \sim 150 \ h^{-1} \text{ kpc}$ reported by [Patton et al. \(2013\)](#), most of the early studies conclude that the galaxies in pairs start to show significant interactions only at $d_p \leq 50 \ h^{-1} \text{ kpc}$ ([Lambas et al. 2003](#); [Ellison et al. 2008, 2011](#); [Scudder et al. 2012](#); [Davies et al. 2015](#)). The much larger critical d_p values revealed in this study is

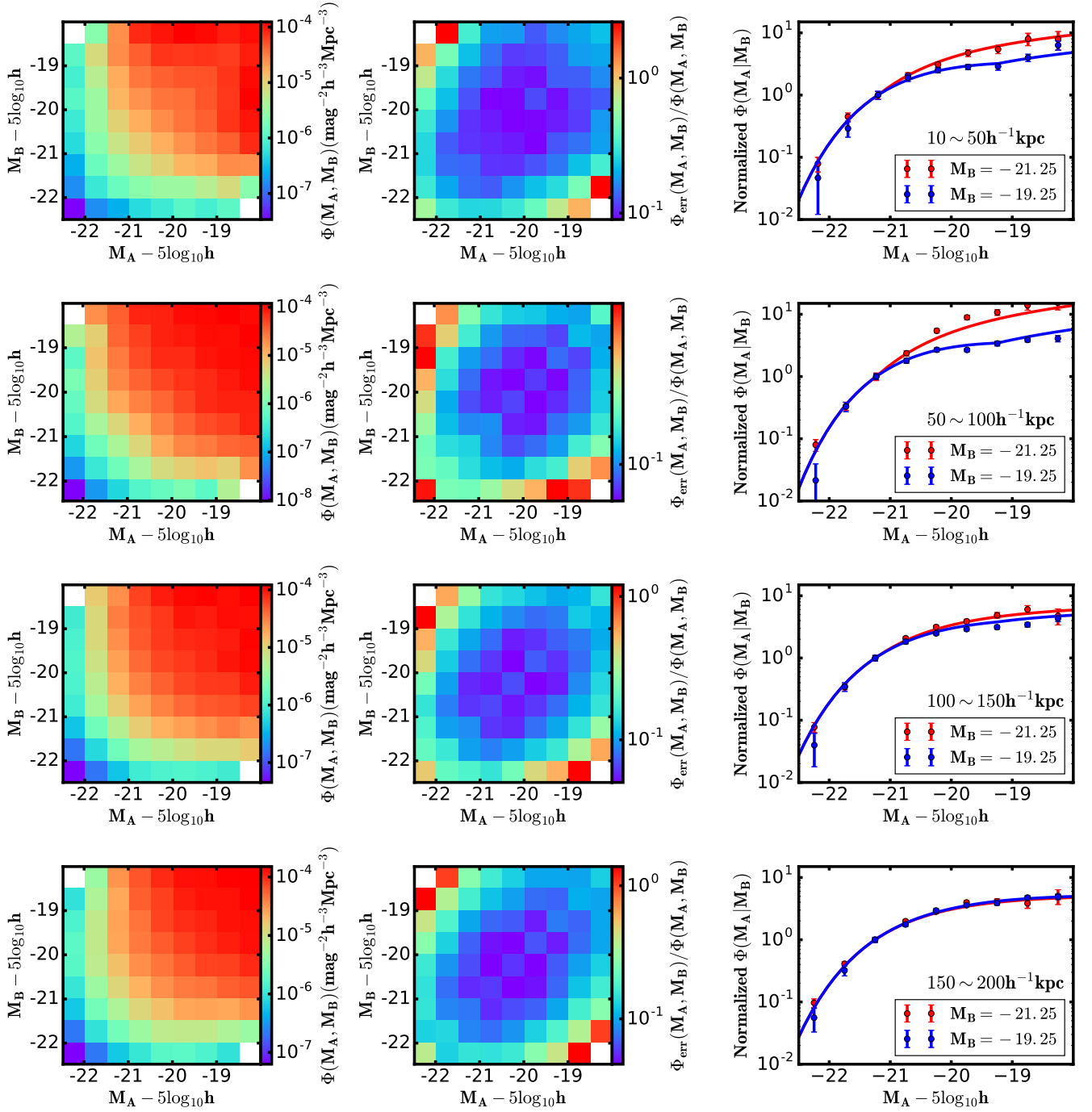


Figure 3. BLFs for different d_p bins. *Left panels:* BLF values. *Middle panels:* relative errors of BLF. *Right panels:* the dots with error bars indicate CLFs $\Phi(M_A|M_B = -21.25)$ and $\Phi(M_A|M_B = -19.25)$, whereas the solid lines show the best fit of Equation 13.

attributed to our statistical approach. Early studies typically compare the physical properties of galaxies in pairs with a control sample (those not in pairs). By control samples, the enhanced star formation in galaxy pairs could be revealed, but the galaxy merging effect, which changes the relative number density of pair members, could not be seen (see further discussion in Section 4.2).

In general, at $d_p \leq 150 h^{-1} \text{ kpc}$, the CLFs of pair members with brighter neighbors [e.g., $\Phi(M_B|M_A = -21.25)$] are biased to distributions with a higher fraction of faint galaxies ($M_B > -20.5$). It means, there are a lower fraction of bright-bright pairs than that expected from a random combination. This bias seems to be the strongest at $50 h^{-1} \text{ kpc} \leq d_p \leq 100 h^{-1} \text{ kpc}$ rather than the smallest d_p bin ($10 h^{-1} \text{ kpc} \leq d_p \leq 50 h^{-1} \text{ kpc}$). Such a complex behavior implies that different mechanisms dominate the galaxy-galaxy interaction within galaxy pairs at different phases (characterized by different d_p values), which will be discussed in Section 4.

3.3. Parametrization of BLF

The non-parametrized BLF maps shown in Figure 3 are neither user-friendly nor easy to understand. Moreover, the CLFs extracted from BLF maps do not contain all the information of the BLFs. To overcome these shortcomings, we further attempt to approximate and parametrize the BLF maps using an analytical formula to describe better and quantify the BLF maps.

It is well known that the LF of galaxies can be well parametrized by a Schechter function (Schechter 1976),

$$\Phi(M) = 0.4 \ln(10) \phi^* 10^{-0.4(M-M^*)(\alpha+1)} \times \exp[-10^{-0.4(M-M^*)}], \quad (12)$$

where ϕ^* is the overall amplitude, M^* and α are the characteristic magnitude and faint-end slope respectively.

Following this convention, we parametrize the BLF of galaxy pairs with,

$$\Phi_{\text{pair}}(M_A, M_B) = [0.4 \ln(10)]^2 \phi_{\text{pair}}^* \times \Phi_{\text{Sch}}(M_A) \Phi_{\text{Sch}}(M_B) X(M_A, M_B), \quad (13)$$

where $\Phi_{\text{Sch}}(M)$ is a Schechter-like function representing the LF shape of single galaxies, and the term $X(M_A, M_B)$ describes the correlation between pair members. More specifically, $\Phi_{\text{Sch}}(M)$ takes the form of Equation 12 but without the density parameter ϕ^* . The density parameter of galaxy pairs is represented by ϕ_{pair}^* in Equation 13.

We parameterize the correlation term $X(M_A, M_B)$ with an assumed form,

$$X(M_A, M_B) = e^{\beta|M_A - M_B|}, \quad (14)$$

where β is the only parameter quantifying the strength of correlation.

For the case of $\beta = 0$, in which $\Phi_{\text{pair}}(M_A, M_B) \propto \Phi_{\text{Sch}}(M_A) \Phi_{\text{Sch}}(M_B)$, there is no correlation between pair members and the BLF degenerates into the product of the LF of single galaxies. In other words, the galaxy pairs are built through a random combination of single galaxies. When $\beta > 0$, the galaxy pairs with large magnitude gap ($|M_A - M_B|$) account for a larger fraction than a random combination. On the contrary, $\beta < 0$ means that the fraction of galaxy pairs with large magnitude gaps is lower. With such a parametrization, we would expect that $\beta \approx 0$ at $d_p > 150 h^{-1} \text{ kpc}$. For the other three d_p intervals, we expect $\beta > 0$, since we have shown in Figure 3 that the brighter galaxies ($M_A = -21.25$) have more faint companions than random combinations, i.e., the galaxy pairs with a larger magnitude gap are more preferred.

We fit BLFs of all sub-samples with Equation 13 using the minimum χ^2 fitting technique. We estimate the uncertainty of each fitting parameter using the 16th and 84th percentiles (half of the interval) of the marginal distribution of the likelihood, which is defined as

$$\mathcal{L} = \exp(-\frac{\chi^2}{2}). \quad (15)$$

First, we fit the BLF of the galaxy pairs within the bin $150 h^{-1} \text{ kpc} \leq d_p \leq 200 h^{-1} \text{ kpc}$, where α , M^* , ϕ_{pair}^* and β are all set as free parameters. As expected, the best fit has $\beta = 0.00 \pm 0.02$, confirming our conjecture that there is no correlation between the pair members within the bin $150 h^{-1} \text{ kpc} \leq d_p \leq 200 h^{-1} \text{ kpc}$. The best fit of the other three parameters are $\phi_{\text{pair}}^* = 2.12 \pm 0.04 \times 10^{-4} h^{-3} \text{ Mpc}^{-3}$, $M^* = -20.71 \pm 0.02$, $\alpha = -1.01 \pm 0.02$ respectively. Next, for the galaxy pairs in the other three d_p intervals, we fix $\alpha = -1.01$ and fit the BLF with M^* , ϕ_{pair}^* and β as free parameters. Since the lower magnitude limit of pair members is only down to -18 mag , if α is also set as a free parameter, it would show strong degeneracy with the characteristic magnitude M^* . Therefore, if we fix α , the change in BLF shape with d_p could be reproduced by the variation of M^* and β , which could also be directly compared to the BLF within the bin $150 h^{-1} \text{ kpc} \leq d_p \leq 200 h^{-1} \text{ kpc}$.

The best fitting parameters of all four BLF maps are listed in Table 2. All four bins have $\chi_{\text{dof}}^2 \sim 1$, indicating that the parametrized BLFs (Equation 13) can well represent the non-parametrized BLF maps shown in Figure 3. As an illustration of the goodness of fit, we also plot two CLFs, $\Phi(M_B|M_A = -21.25)$ and $\Phi(M_B|M_A = -19.25)$, deduced from the best fitting

Table 2. The best fitting parameters and their uncertainties in Equation 13 for the BLFs in four different d_p intervals.

| d_p (kpc) | N_{pair} | ϕ_{pair}^* ($10^{-4} h^{-3} \text{ Mpc}^{-3}$) | M^* | α | β | χ_{dof}^2 |
|----------------|-------------------|---|-------------------|------------------|-----------------|-----------------------|
| 10 \sim 50 | 6826 | 1.26 ± 0.04 | -20.58 ± 0.02 | — | 0.21 ± 0.03 | 1.73 |
| 50 \sim 100 | 11314 | 1.78 ± 0.05 | -20.48 ± 0.01 | — | 0.24 ± 0.02 | 1.01 |
| 100 \sim 150 | 13657 | 1.86 ± 0.04 | -20.68 ± 0.01 | — | 0.05 ± 0.02 | 0.99 |
| 150 \sim 200 | 14713 | 2.12 ± 0.04 | -20.71 ± 0.02 | -1.01 ± 0.02 | 0.00 ± 0.02 | 0.79 |

parameters, as solid lines in the right panels of Figure 3 for comparison.

We show the best fitting parameters β and M^* as functions of d_p in the top two panels of Figure 4. With the decrease of d_p , β shows an increasing trend until d_p reaches $50 h^{-1} \text{ kpc}$, then stays unchanged. The variation of M^* is similar, which gradually increases (becomes fainter) with decreasing d_p and then drops (becomes brighter) within the innermost bin ($10 h^{-1} \text{ kpc} \leq d_p \leq 50 h^{-1} \text{ kpc}$). The increasing trend of β implies that the galaxy-galaxy interaction gets stronger when they get closer. Because of the correlation term β , we remind that the physical implication of M^* is not as straightforward as that in the LF of single galaxies. Therefore, the variation of the best fitting parameters listed in Table 2 cannot be over-interpreted. We will discuss the physical implications of these BLF results in more details in Section 4.

3.4. Univariate Luminosity Function and Number Density of Galaxy Pairs

From the BLF shown in Figure 3, we can obtain the ULF of galaxy pairs through integrating the magnitudes of one member,

$$\Phi(M_A) = \int_{-22.5}^{-18.0} \Phi_{\text{pair}}(M_A, M_B) dM_B. \quad (16)$$

Here, the integration can only be performed in the magnitude range where the BLF has been calculated. Namely, the galaxy pairs here have been strictly defined as those both of whose members are in the magnitude range of $-22.5 \leq M_r \leq -18.0$.

In Figure 5, we show the resulting ULFs of the galaxy pairs within four different d_p bins. We also fit these ULFs with a Schechter function, and the resultant fittings are shown as the corresponding solid curves in Figure 5. The fitting parameters of the Schechter function are also listed in Table 3. Since our galaxy pair sample is a subsample of the SDSS MGS, the ULFs can be directly compared with the global LF of SDSS galaxies (Blanton et al. 2003a). Because the galaxy pair is one kind of environments for a galaxy, the ULF of galaxy pairs is expected to be different from the global LF of galaxies. This is indeed the

Table 3. The best fitting parameters and their uncertainties of the ULFs in four different d_p intervals.

| d_p (kpc) | ϕ^* ($10^{-4} h^{-3} \text{ Mpc}^{-3}$) | M^* | α |
|----------------|---|-------------------|------------------|
| 10 \sim 50 | 6.59 ± 0.06 | -20.58 ± 0.08 | -0.95 ± 0.06 |
| 50 \sim 100 | 8.01 ± 0.06 | -20.61 ± 0.07 | -0.96 ± 0.05 |
| 100 \sim 150 | 9.57 ± 0.05 | -20.51 ± 0.05 | -0.85 ± 0.04 |
| 150 \sim 200 | 10.73 ± 0.06 | -20.52 ± 0.05 | -0.92 ± 0.04 |

case. For example, for the galaxy pairs within the widest d_p bin ($150 h^{-1} \text{ kpc} \leq d_p \leq 200 h^{-1} \text{ kpc}$), where even none galaxy-galaxy interaction effects have been detected in the BLF measurement, their ULF still shows a brighter characteristic magnitude -20.52 and a shallower faint-end slope -0.92 than the general SDSS galaxies ($M_* = -20.44, \alpha = -1.04$). Such behavior is consistent with the earlier findings for the general trend of the environmental dependence of the LF of galaxies (e.g. McNaught-Roberts et al. 2014; Alpaslan et al. 2015).

The shapes of the ULFs within four different d_p bins are quite similar with values of M^* and α overlapping each other inside $1\text{-}\sigma$ uncertainties. The similarities of the ULFs contrast with the BLF behaviors, which reveals different physical mechanisms behind two types of LFs. Generally, BLFs describe the galaxy interactions between pair members, while the ULFs are further correlated with the global environment of galaxy pairs. The weak dependence of the ULFs on d_p implies that the global environments of different types of galaxy pairs are quite similar.

The amplitude of the BLFs/ULFs tells us the number density of galaxy pairs. As shown by ϕ_{pair}^* and ϕ^* in Table 2 and 3, the global number densities of paired galaxies in the SDSS volume are quite similar within four different d_p intervals. These characteristics of the global number densities have already been seen in the flat d_p distribution of our galaxy pair sample after the correction of incompleteness (red dashed line in the bottom left panel of Figure 1). On the other hand, since the local volumes occupied by galaxy pair themselves are smaller for smaller d_p values, the resulting local number density of the galaxies in close pairs is higher than that in wide

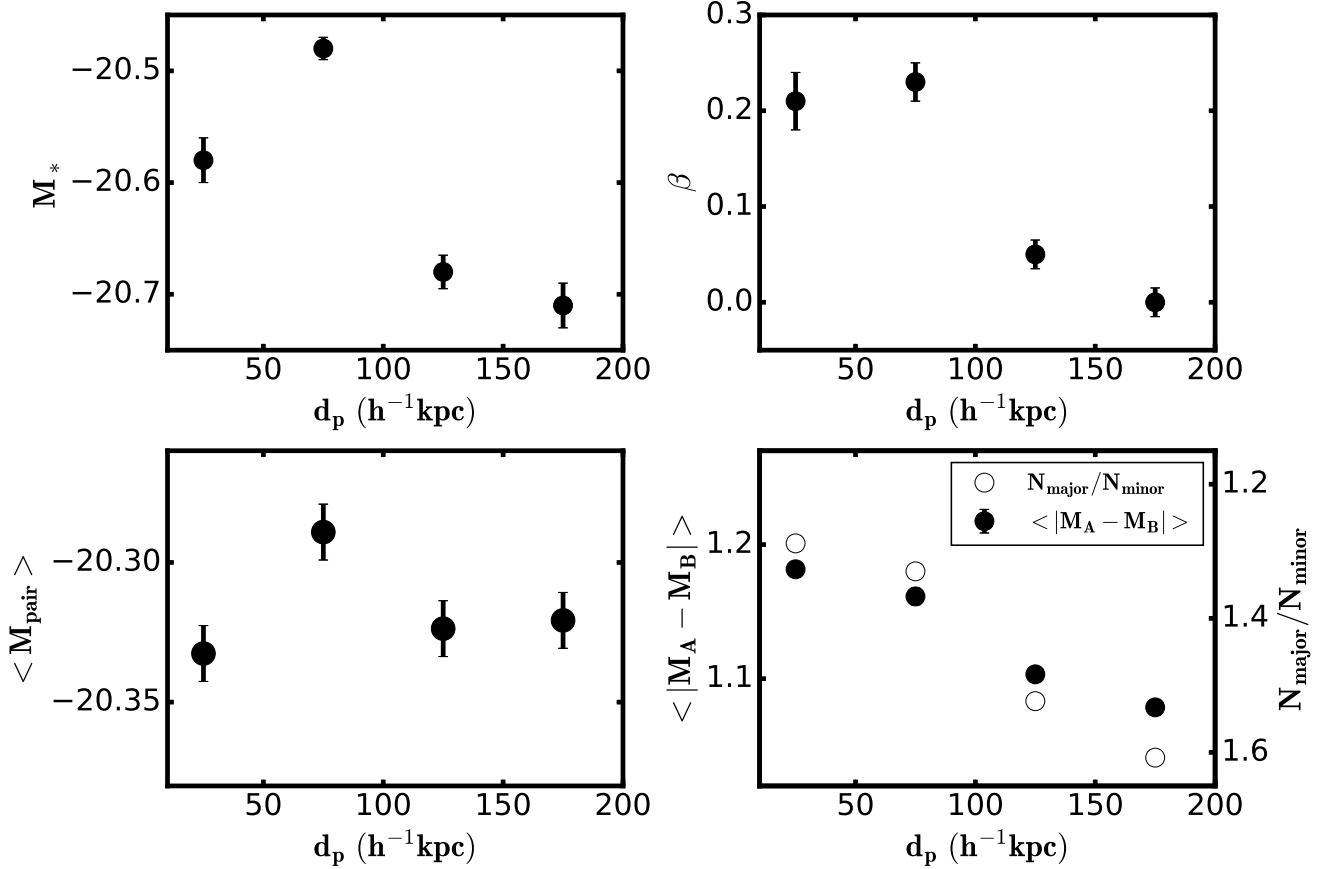


Figure 4. Parameterization of BLF variation. *Top panels:* the best fitting values in Equation 13 when α is fixed, including the character magnitude M^* (top left) and correlation strength β (top right). *Bottom panels:* the statistical quantities of our galaxy pair sample, including the mean total magnitude of the galaxy pairs $\langle M_{\text{pair}} \rangle$ (bottom left), mean magnitude gap of the galaxy pairs $\langle |M_A - M_B| \rangle$ and number density ratio of the major merger pairs to minor merger pairs $N_{\text{major}}/N_{\text{minor}}$ (bottom right). In the bottom right panel, the values of $\langle |M_A - M_B| \rangle$ and $N_{\text{major}}/N_{\text{minor}}$ are labelled on the left and right y -axis respectively.

pairs. The different behaviors of the global and local number densities of paired galaxies exhibit the galaxy clustering effect, where galaxies are more clustered in smaller d_p scales.²

By integrating the BLFs, we can further estimate the number densities of galaxy pairs with any specific magnitude configuration. For example, we have estimated from the BLF map that the number density of galaxies in the range of $-19 \leq M_r \leq -21.5$ and locating in the the galaxy pairs with $\Delta M_r \leq 1$ and $10 h^{-1} \text{ kpc} \leq d_p \leq 50 h^{-1} \text{ kpc}$ equals to $n = 4.59 \times 10^{-3} h^{-3} \text{ Mpc}^{-3}$. Accounting the number density of the general SDSS galaxies in the same magnitude range ($\sim 0.015 h^{-3} \text{ Mpc}^{-3}$ from Blanton et al. 2003b), we conclude that 3.06% of

the SDSS galaxies locate in galaxy pairs with $\Delta M_r < 1$ and $10 h^{-1} \text{ kpc} \leq d_p \leq 50 h^{-1} \text{ kpc}$. This result is consistent with the early estimation of the pair fraction from the ULF of galaxy pairs ($\sim 1.6\%$ Domingue et al. 2009), where the galaxy pairs are limited to those with $\Delta M_{K_s} < 1$ and $5 h^{-1} \text{ kpc} \leq d_p \leq 20 h^{-1} \text{ kpc}$.

4. PHYSICAL INTERPRETATION OF THE BLF VARIATION

In this section, we first quantify the BLF dependence on d_p by defining two new statistical quantities (Section 4.1) and then discuss their variation with physically motivated toy models (Section 4.2 and 4.3).

4.1. $\langle M_{\text{pair}} \rangle$ and $\langle |M_A - M_B| \rangle$ of Galaxy Pairs

For individual galaxy pairs, the total magnitude M_{pair} and magnitude gap $|M_A - M_B|$ are sufficient to fully describe the magnitude configuration of its members. For statistical samples, the mean values of these two quantities, $\langle |M_A - M_B| \rangle$ and $\langle M_{\text{pair}} \rangle$ present a first order

² Because of the limited number of galaxies and complicated selection effects, the studies of galaxy clustering effects at very small scales (e.g., $d_p < 100 h^{-1} \text{ kpc}$) are very limited (e.g. Guo et al. 2012).

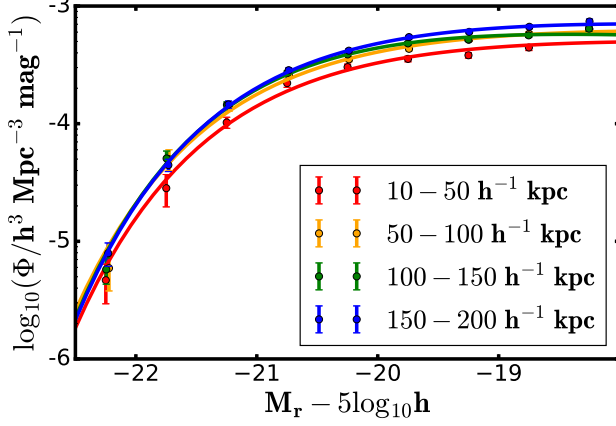


Figure 5. The ULFs of four subsamples. *Dots*: the ULFs derived from BLFs. *Solid Lines*: the best fits by Schechter Function.

description of the BLF shape. Specifically, $\langle M_{\text{pair}} \rangle$ describes the average total magnitude of pairs, whereas $\langle |M_A - M_B| \rangle$ mainly reflects the magnitude configuration. In addition, $|M_A - M_B|$ is also used to define the merging type of each galaxy pair, if the mass-to-light ratio of pair members are assumed to be the same. Following convention, we define the major and minor merger pairs according to the criteria $1/3 \leq L_A/L_B \leq 3$. Typically, larger $\langle |M_A - M_B| \rangle$ indicate a lower fraction of major merger pairs in the galaxy pair sample.

We calculate the average total magnitude $\langle M_{\text{pair}} \rangle$ and the average magnitude gap $\langle |M_A - M_B| \rangle$ of each subsample from the BLF maps. We show $\langle M_{\text{pair}} \rangle$ and $\langle |M_A - M_B| \rangle$ as functions of d_p in lower two panels of Figure 4, where the number density ratio of the major merger pairs to minor merger pairs $N_{\text{major}}/N_{\text{minor}}$ is also incorporated in the bottom right panel.

As d_p decreases, $\langle |M_A - M_B| \rangle$ increases ($N_{\text{major}}/N_{\text{minor}}$ decreases) monotonously. Such a behavior is very similar to the trend of β shown in the top right panel. By contrast, the variation of $\langle M_{\text{pair}} \rangle$ is similar to the trend of M^* , which increases gradually and then drops within the innermost d_p bin.

The variation of the BLFs and the BLF parameters as functions of d_p shown in Figure 3 and 4 implies that there are three *phases* during the galaxy pair evolution. In the beginning, i.e., the first phase, when the distance of two pair members is very large ($d_p \geq 150 h^{-1}$ kpc), there is little interaction between them, and the BLF of galaxy pairs degenerates into the LF of single galaxies (bottom panels of Figure 3). In the second phase, when $50 h^{-1}$ kpc $\leq d_p \leq 150 h^{-1}$ kpc, both the fraction of the major merger pairs and the average total luminosity of galaxy pairs systematically decrease with decreasing d_p . These results imply that the interaction

drives the number of luminous major merger pairs successively to drop. This behavior resembles the merging process induced by dynamic friction where the merging time-scale of the massive major merger pairs is shorter than others (see further discussion in Section 4.2). For the third phase ($10 h^{-1}$ kpc $\leq d_p \leq 50 h^{-1}$ kpc), the effect of dynamic friction still remains ($\langle |M_A - M_B| \rangle$ keeps increasing), whereas another effect in turn brightens the average total luminosity of galaxy pairs. In close pairs (e.g. $d_p < 50 h^{-1}$ kpc), it has long been known that the close interaction enhances the star formation so that also brightens the luminosity of the paired galaxies (Ellison et al. 2008; Scudder et al. 2012; Patton et al. 2013; Davies et al. 2015, see further discussion in Section 4.3).

4.2. Merging Time-scale

Once the galaxy pairs are in bound orbits, the dynamical friction will drive the pair members to approach each other and finally merge. The detailed merging process of a specific galaxy pair includes a very complex chain of events, and the merging time-scale is related to many details, e.g., the galaxy orbit, mass, angular momentum and internal structure of the paired galaxies etc. (Colpi et al. 1999; Boylan-Kolchin et al. 2008; Lotz et al. 2010a,b). However, numerical simulations have shown that the merging time-scale of galaxy pairs mainly depends on the masses of pair members, and the typical merging time-scale (from a bound orbit to the final merge) is about $\sim 1-2$ Gyr (e.g., Jiang et al. 2014).

Many studies have shown that galaxy pairs with comparable stellar masses (i.e., major merger pairs), merge more quickly than the minor merger ones (e.g. Boylan-Kolchin et al. 2008). This effect is typically parameterized by

$$T_m \sim \left(\frac{M_{h,1}}{M_{h,2}} \right)^a$$

where $M_{h,1}$ and $M_{h,2}$ are the halo masses of the primary and secondary galaxies respectively. Although the consensus is that $a > 0$, the index a spans a wide range (from ~ 0.4 to ~ 1.3) in different studies (Lacey & Cole 1994; Colpi 1998; Boylan-Kolchin et al. 2008). Besides the mass ratio M_1/M_2 , the merging time-scale is also correlated with the mass of primary galaxy (Jiang et al. 2014). Namely, a more massive galaxy pair would also have a shorter T_m ($T_m \sim M_{h,1}^{-1/3}$ in Jiang et al. 2014).

Taking all these factors into account, and assuming a constant dark matter halo mass-to-light ratio of galaxies, we parameterize T_m as a function of the luminosities of pair members,

$$T_m(L_A, L_B) \sim T_m(L_1, L_2) \sim \left(\frac{L_1}{L_2} \right)^a (L_1 + L_2)^b \quad (17)$$

where L_1 and L_2 represent the luminosities of the primary and secondary members, a and b are free parameters.

In a hierarchical clustering universe, galaxy pairs bound and merge continuously. We assume that galaxy pairs are formed through a random combination of field/single galaxies when their two members approach each other at a critical distance (e.g., $d_p \sim 175 h^{-1} \text{ kpc}$). Thus, the birth rate of galaxy pairs is proportional to the product of the number densities of two pair members,

$$\dot{\Phi}(L_A, L_B) \propto \Phi_0(L_A)\Phi_0(L_B) \quad (18)$$

where Φ_0 is the LF of single/field galaxies. As we have shown in Section 3.3, the galaxy pairs within the bin $150 h^{-1} \text{ kpc} \leq d_p \leq 200 h^{-1} \text{ kpc}$ show no internal correlation and can be viewed as random combinations of single galaxies. The excellent fitting of Equation 13 for the BLF of galaxy pairs within this d_p interval tells us that the LF of single galaxies Φ_0 to be forming galaxy pairs could be parameterized by a Schechter function with $M^* = -20.73$ and $\alpha = -1.01$.

Then, the observed number density of galaxy pairs with a given configuration is further proportional to their lifespan, i.e., the merging time-scale T_m ,

$$N(L_A, L_B) \propto \Phi_0(L_A)\Phi_0(L_B)T_m(L_A, L_B). \quad (19)$$

These galaxy pairs would span a wide distribution of projected distance d_p , ranging from d_{\min} to d_{\max} , where d_{\min} and d_{\max} are the minimum and maximum projected distances between pair members. We denote the number density of galaxy pairs at a certain d_p as $N(L_A, L_B, d_p)$, and assume that the $N(L_A, L_B, d_p)$ distribution follows a linear relation with d_p . Namely, once we have constraints on the number density of galaxy pairs at both d_{\min} and d_{\max} , the $N(L_A, L_B, d_p)$ distribution could be easily figured out.

For the galaxy pairs at d_{\max} , we know that their relative number density is independent of the merging time-scale and is only determined by their birth rate, i.e.,

$$N(L_A, L_B, d_{\max}) \propto \dot{\Phi}_{L_A, L_B} \propto \Phi_0(L_A) * \Phi_0(L_B). \quad (20)$$

Moreover, with the key assumption of a linear $N(L_A, L_B, d_p)$ distribution, the number density of galaxy pairs at d_{\min} , $N(L_A, L_B, d_{\min})$ could be estimated through the relation

$$N(L_A, L_B) = 0.5 \frac{N(L_A, L_B, d_{\max}) + N(L_A, L_B, d_{\min})}{(d_{\max} - d_{\min})}. \quad (21)$$

So far, the last piece of the $N(L_A, L_B, d_p)$ distribution is the normalization constant of Equation 19 and 20, which also determines the global d_p distribution of

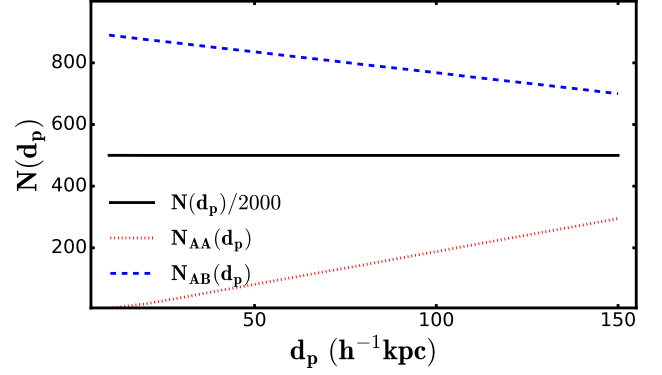


Figure 6. The d_p distribution of mock galaxy pairs generated from Monte-Carlo simulation (see the text in Section 4.2 for details). The black solid line shows the d_p distribution of all 15,000,000 mock pairs, where the y-axis values have been divided by 200 for clarity. The red dotted and blue dashed line show the d_p distribution of galaxy pair AA ($-20.75 \pm 0.25, -20.75 \pm 0.25$) and AB ($-20.75 \pm 0.25, -18.75 \pm 0.25$) respectively.

galaxy pairs. Motivated by our galaxy pair sample, a reasonable assumption on the global d_p distribution is a flat distribution (see the red dotted line in the bottom left panel of Figure 1).

In practice, for a given parameterization of merging time-scale (Equation 17), we use a Monte Carlo simulation to generate 15,000,000 mock galaxy pairs using Equation 17 and 19, where Φ_0 takes the Schechter function with $M^* = -20.73$ and $\alpha = -1.01$. As for the observed sample, the mock galaxies are set in the magnitude range of -18.0 to -22.5 mag and d_p is set in the range of $d_{\min} = 10 h^{-1} \text{ kpc}$ to $d_{\max} = 150 h^{-1} \text{ kpc}$. We divide the mock pairs into 15 d_p bins with a bin width of $10 h^{-1} \text{ kpc}$. Since the mock galaxy pair sample has been assumed to have a flat d_p distribution, the number of mock pairs within each d_p bin is therefore $\sim 1,000,000$. For galaxy pairs with specific configuration (L_A, L_B) , their numbers within the d_{\max} bin ($145 - 155 h^{-1} \text{ kpc}$) follow the distribution of a random combination of single galaxies as shown by Equation 20. Then, the number of the galaxy pairs within the d_{\min} bin is calculated using Equation 21. Finally, the number of mock pairs within any given d_p bin could be easily interpolated from $N(L_A, L_B, d_{\max})$ and $N(L_A, L_B, d_{\min})$.

To give an example, we show the mock galaxy pairs with two specific magnitude configuration ($-20.75 \pm 0.25, -20.75 \pm 0.25$) and ($-20.75 \pm 0.25, -18.75 \pm 0.25$). These represent the major and minor merger pairs respectively and are denoted as AA and AB below. Here, we take the modeling for the merging time-scale (Equation 17) of $a = 0.40$ and $b = -0.33$ as an

illustration. First, among 15,000,000 mock pairs, there are 2,264 AA and 12,126 AB respectively (Equation 19). Then, with Equation 20, we know that there are 302 AA and 713 AB within the d_{\max} bin. Using Equation 21, we obtain that there are 4 AA and 904 AB within the d_{\min} bin. Finally, the numbers of AA and AB within all d_p bins are obtained from linear interpretation, which is illustrated in Figure 6. As can be seen, because of their different merging time-scales, AA (major merger pairs) show a significant different d_p distribution from AB (minor merger pairs). In our modeling, because of their longer merging time-scale, there is an increasing fraction of minor merger pair in inner d_p regions. This phenomenon is consistent with a scenario, that the minor merger pairs experience more orbits before coalescing and are more frequently observed in the inner d_p regions (van den Bosch et al. 1999).

The toy modeling we presented above may not be enough to characterize all the variations of BLFs. Therefore, we do not attempt to model the variation of the exact shape of BLF but to focus on the general trends of the BLF parameters as functions of d_p . Specifically, we model the trends of $\langle |M_A - M_B| \rangle$, $\langle M_{\text{pair}} \rangle$ and $N_{\text{major}}/N_{\text{minor}}$, then compare them with the observational results already shown in Section 4.1.

We first take two sets of parameterizations of T_m from Lacey & Cole (1994); Colpi (1998), i.e., ($a = 1.0, b = 0$) and ($a = 0.4, b = 0$). The results are plotted as red dotted and green dot-dashed lines in each panel of Figure 7. In these two models, luminosity/mass ratio is the only component of T_m . A positive a means that the merging time-scale of minor merger pairs is larger than the major merger ones, which naturally results in a larger average $\langle |M_A - M_B| \rangle$ and a higher fraction of minor merger pairs. Moreover, both two models predict the trend of increasing $\langle |M_A - M_B| \rangle$ (decreasing $N_{\text{major}}/N_{\text{minor}}$) with the decreasing d_p . This trend is steeper for larger a values. Moreover, in the $a > 0$ models, the pairs with very bright primary galaxies are also preferred (because they are mainly minor merge pairs), which in turn results in a brightening of $\langle M_{\text{pair}} \rangle$. This decreasing trend of $\langle M_{\text{pair}} \rangle$ with decreasing d_p is in conflict with observations. The results shown above indicate that although smaller a is preferred by the observations, this simple parameterization is not enough to explain all the observed BLF trends.

Next, we take both the luminosity/mass ratio and total luminosity/mass into account. Following Jiang et al. (2014), we take $a = 1.0, b = -0.33$ and the results are shown as the blue dashed line in Figure 7. When $b < 0$, the merging time-scale of brighter galaxy pairs is smaller, which results in a fainter $\langle M_{\text{pair}} \rangle$ than the

corresponding $b = 0$ model. However, in this model, the effect of $b = -0.33$ seems not enough to balance the effect of $a = 1.0$ on the predicted $\langle M_{\text{pair}} \rangle$ trend.

So far, all these three models inferred from literature could not reproduce the general trends of $\langle M_{\text{pair}} \rangle$ and $\langle |M_A - M_B| \rangle$ simultaneously. A natural conclusion from comparison of these three models is that a smaller positive a value and negative b value would be more consistent with observations, which leads to our final test model with $a = 0.4$ and $b = -0.33$. The model predictions are shown as the black solid lines in Figure 7. This model reproduces all the global trends of $\langle |M_A - M_B| \rangle$ and $N_{\text{major}}/N_{\text{minor}}$. For $\langle M_{\text{pair}} \rangle$, this model also predicts the general trend well, except the smallest d_p bin where a jump (brightening) of $\langle M_{\text{pair}} \rangle$ is clearly seen.

We emphasize that the fourth model with $a = 0.4$ and $b = -0.33$ is only a test and not a fitting of the observed trends of $\langle M_{\text{pair}} \rangle$ and $\langle |M_A - M_B| \rangle$. As already implied from four test models, there is certain degeneracy of model predictions between the model parameters a and b . The discrepancy between the observed and modeled trends of $\langle M_{\text{pair}} \rangle$ and $\langle |M_A - M_B| \rangle$ could be further alleviated by taking either a smaller positive a value or a more negative b value. Nevertheless, none of the parameters (a or b) alone can reproduce the observed $\langle M_{\text{pair}} \rangle$ and $\langle |M_A - M_B| \rangle$ trends simultaneously.

4.3. Enhanced Star Formation in Close-Pair Phase

As we have shown in Section 4.2, the merging time-scale effect could well explain most of the BLF variation features, except that the average total luminosity of galaxy pairs within the bin $10 h^{-1} \text{ kpc} \leq d_p \leq 50 h^{-1} \text{ kpc}$ becomes significantly brighter. Such a feature is consistent with the scenario that there is enhanced star formation in close pairs (Ellison et al. 2008), which has not been taken into account so far. In this section, we discuss how star formation enhancement induces galaxy brightening, and thus changes the BLF of galaxy pairs. For the sake of brevity, we name the galaxy pairs within the bin $10 h^{-1} \text{ kpc} \leq d_p \leq 50 h^{-1} \text{ kpc}$ as close pairs below.

Quantitatively, our BLF measurements show that the average total magnitude ($\langle M_{\text{pair}} \rangle$) of close pairs is 0.043 mag brighter than the galaxy pairs within the bin $50 h^{-1} \text{ kpc} \leq d_p \leq 100 h^{-1} \text{ kpc}$. However, besides the enhanced star formation effect, the magnitude configurations of close pairs may have been further altered by the merging time-scale effect compared to those within the bin $50 h^{-1} \text{ kpc} \leq d_p \leq 100 h^{-1} \text{ kpc}$ (see the solid line in the top left panel of Figure 7). Therefore, the average brightening of the galaxies in the close-pair phase, $\Delta M_r \sim 0.04$, is quite conservative.

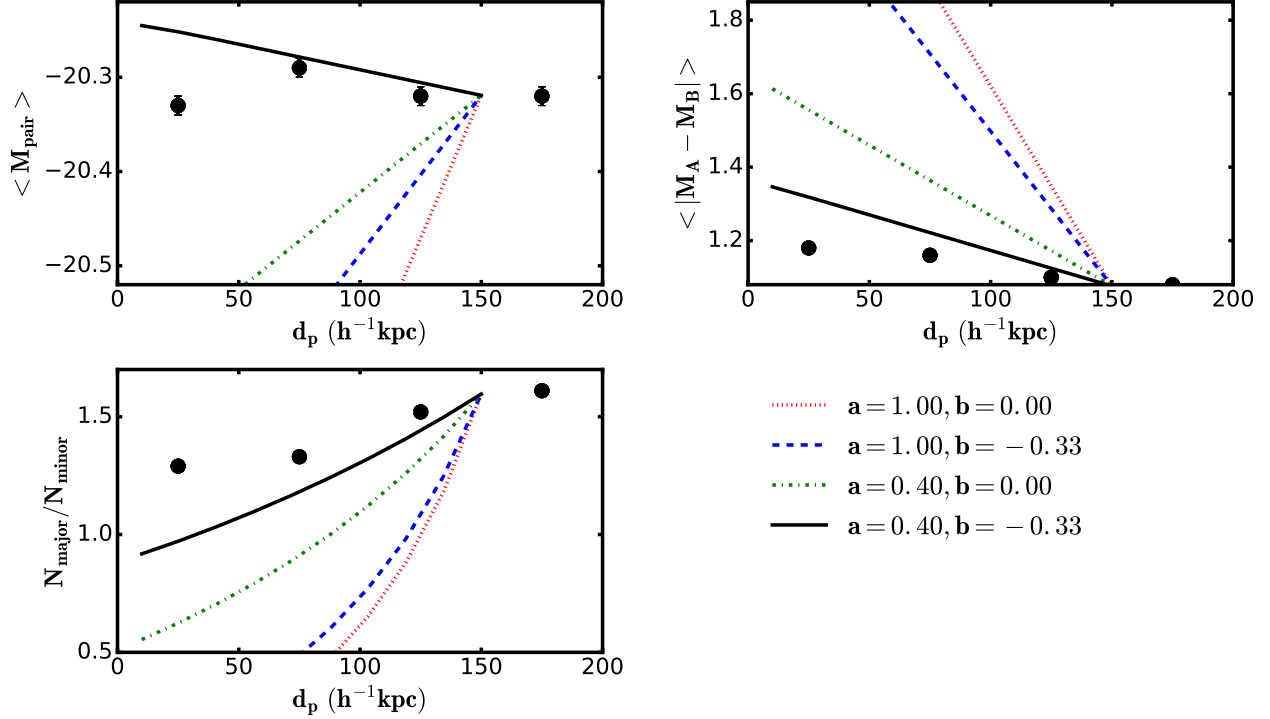


Figure 7. Modelling of the BLF variation with d_p . *Black dots:* the observational values of the BLF parameters, including the mean total magnitude (*top left*), mean magnitude gap (*top right*) and number density ratio between major merger pairs and minor merger pairs (*bottom left*). *Lines:* BLF variation predicted by the merging time-scale model (Section 4.2), where different lines indicate different merging time-scales parameterized by Equation 17.

On the other hand, the SFR enhancement of close pairs could be directly estimated from data. To do that, we take the total SFR and stellar mass of the galaxies in our galaxy pair sample from GALEX-SDSS-WISE Legacy Catalog 2 (GSWLC-2) (Salim et al. 2016, 2018). We define the galaxies which satisfy $\text{SFR}_0/M_\star > 10^{-11} \text{yr}^{-1}$ as star-forming galaxies (Salim et al. 2018). We show the fraction of star-forming galaxies and their mean specific SFR ($\text{sSFR} = \text{SFR}/M_\star$) as a function of d_p for four subsamples of galaxy pairs in Figure 8. As shown in that figure, both the fraction of star-forming galaxies and their average sSFR are roughly constant for paired galaxies when $d_p \geq 50 h^{-1} \text{kpc}$. While for close pairs, both of them show increments. The increase of the fraction of the star-forming galaxies is very weak ($\sim 2\%$), while the enhancement of the sSFR is very significant ($\sim 40\%$). Such a result confirms the scenario that the star formation efficiency of the gas-rich galaxies is significantly enriched when galaxies are in close-pair phase. The relative enhancement of the SFR we get ($\sim 40\%$) is also consistent with many earlier studies (Ellison et al. 2008; Scudder et al. 2012; Patton et al. 2013; Davies et al. 2015).

For a galaxy with ‘original’ stellar mass of M_\star^3 , the magnitude in r -band brightened by the enhanced star formation could be parametrized as follows,

$$\Delta M_r = -2.5 \log_{10} \frac{L_{r,\text{new}} + L_{r,0}}{L_{r,0}} = -2.5 \log_{10} \left(1 + \frac{\Delta M_\star / \Upsilon_{r,n}}{M_\star / \Upsilon_{r,0}} \right) \quad (22)$$

where $L_{r,0}$ is the ‘original’ luminosity of the galaxy, ΔM_\star and $L_{r,\text{new}}$ are the stellar mass and luminosity of the newborn stars, whereas $\Upsilon_{r,0}$ and $\Upsilon_{r,n}$ are the r -band stellar mass-to-light ratio of the ‘original’ stellar populations and newborn stars respectively. The stellar mass of the newborn stars could be further parametrized by the product of the average enhanced star formation rate ΔSFR and its duration time τ , i.e. $\Delta M_\star = \Delta \text{SFR} \times \tau$. However, since the amount of star formation induced by the galaxy pair environment involves many complex factors (e.g. stellar mass, gas fraction, orbit etc.), it is non-trivial to determine either ΔSFR or τ for individual galaxies in pairs.

³ Here, ‘original’ means that if there is no enhanced star formation, i.e. the case that the galaxy is not in the galaxy pair environment.

From a statistical point of view, we assume that ΔSFR is caused by the increased star formation efficiency and parametrize it with a SFR enhancement strength f_Δ ,

$$f_\Delta = \frac{\Delta\text{SFR}}{\text{SFR}_0} = \frac{\Delta\text{sSFR}}{\text{sSFR}_0} \quad (23)$$

where SFR_0 and sSFR_0 are the ‘original’ SFR and sSFR of galaxies respectively. With this parametrization, only the star-forming(gas-rich) galaxies would show enhanced star formation, while the passive galaxies(gas-poor, $\text{SFR}_0=0$) would not. Thus, we have

$$\Delta M_{r,L} = -2.5 \log_{10}(1 + f_\Delta \tau * \text{sSFR}_0 \frac{\Upsilon_{r,0}}{\Upsilon_{r,n}}) \quad (24)$$

$$\Delta M_{r,E} = 0$$

for late(star-forming) and early(passive) type galaxies respectively. It is well known that the sSFR of local star-forming galaxies only show a weak dependence on their stellar mass. For simplicity, we take $\text{sSFR}_0 = 1.45 \times 10^{-10} \text{yr}^{-1}$, which is the mean value of the paired galaxies within the bin $150 \leq d_p \leq 200 h^{-1} \text{kpc}$.

According to Figure 8, we take the fact that the enhanced star formation only happens in star-forming galaxies in close-pair phase. The fraction of star-forming galaxies is about 50% and the enhancement strength f_Δ equals to 0.4. We estimate the mass-to-light ratio($\Upsilon_{r,n}$) of the newborn stars using the stellar population synthesis model of [Bruzual & Charlot \(2003\)](#), where a continuous and constant star formation process and the Salpeter initial mass function are adopted. We calculate $\Upsilon_{r,n}$ as a function of duration time τ , e.g., $\Upsilon_{r,n} = 0.19$ for $\tau = 0.2 \text{ Gyr}$. For $\Upsilon_{r,0}$ of the ‘original’ galaxies, we take the approximation from [Blanton et al. \(2003b\)](#), where a typical color $g - r \sim 0.4$ of star-forming galaxy corresponds to a mass-to-light ratio $\Upsilon_{r,0} \sim 1.35$ ([Bell et al. 2003](#)).

With all the above prescriptions, we can estimate the duration time τ of the SFR enhancement from the average brightening magnitude $\Delta\bar{M}_r$ of pair members in close pairs using Equation 24. We show $\Delta\bar{M}_r$ as a function of τ as the solid line in Figure 9. As can be seen, for $\Delta\bar{M}_r \geq 0.04 \text{mag}$, the duration of the enhanced star formation is as long as 0.2 Gyr.

The duration time $\tau \sim 0.2 \text{ Gyr}$ we have shown above is the average time that the close pairs have already experienced for the enhanced star formation phase. Statistically, the time-scale of the SFR enhancement phase would be two times more, i.e., 0.4 Gyr. Considering that the brightening magnitude we use is quite conservative, such a result seems consistent within uncertainties with numerical simulation, where the pair phase with significantly enhanced star formation lasts for about 0.1 – 0.5 Gyr ([Cox et al. 2008](#)).

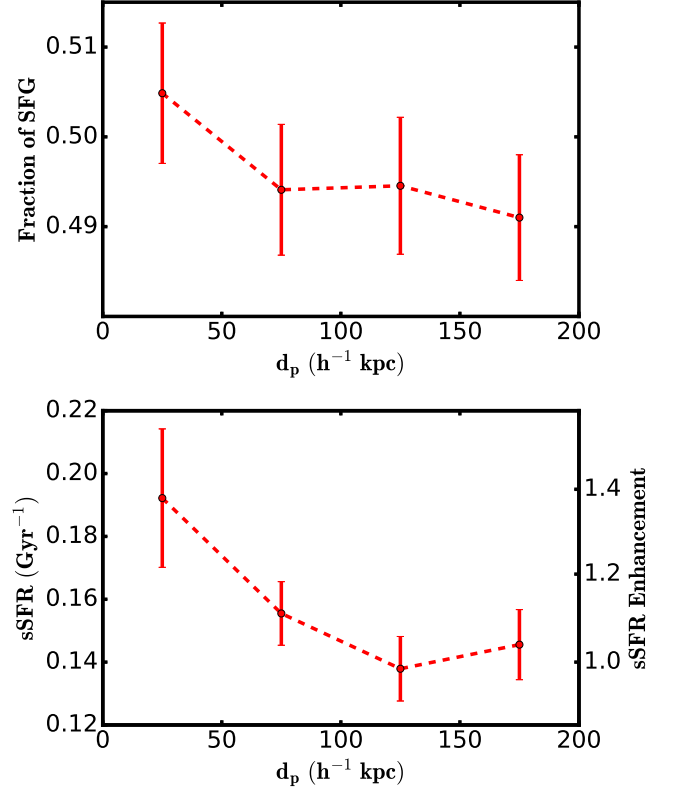


Figure 8. *Top panel:* the fraction of star-forming galaxy as a function of d_p for paired galaxies. *Bottom panel:* the mean sSFR as a function of d_p , see the text in Section 4.3 for details.

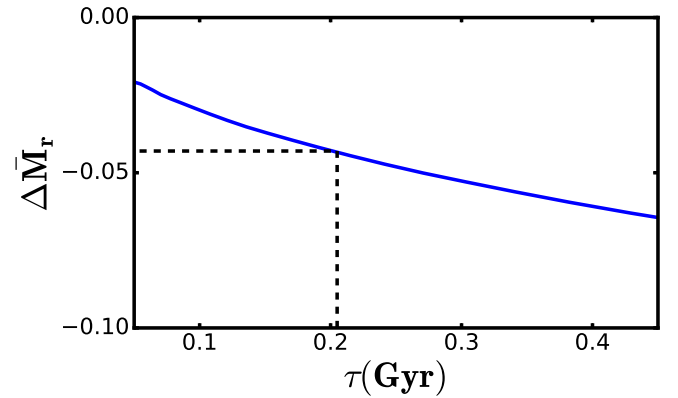


Figure 9. *Blue solid line:* the average brightening magnitude of pair members as a function of τ calculated from Equation 24. *Black dashed line:* the lower limit of the average brightening of r -band magnitude of the close pairs and its corresponding τ .

4.4. Discussion

In Section 4.2 and 4.3, we have shown that the global trend of the BLFs presented in Section 4.1 could be quantitatively explained by two different physical mechanisms, the merging time-scale effect (Section 4.2) and the enhanced star formation in close-pair phase (Section 4.3). However, some details of the model need to be further examined.

For the merging effect of galaxy pairs, first, we emphasize, that we adopt the relative values of the merging time-scales that have been inferred from our modeling, instead of the absolute values. Second, in a physical galaxy pair, it is the host halo mass rather than the galaxy luminosity that is the dominating factor of the merging time-scale, although the galaxy luminosity is a good proxy of its host halo mass (Tinker et al. 2005; Mandelbaum et al. 2006; Velandier et al. 2014). Besides, the dark matter halo mass-to-light ratio of galaxies is not a constant but a non-linear relation of galaxy luminosity (Mandelbaum et al. 2006). Therefore, although both the analytical formula and the parameter values of the merging time-scale used in our modeling are inferred from the simulation results, we may not make a one-to-one comparison with numerical simulations. Third, in our modeling, we have assumed a linear distribution of d_p for all configurations of galaxy pairs, which is too simplistic.

More importantly, our merging time-scale model is only built with a statistical approach, where only the relative number densities of galaxy pairs have been addressed. Apparently, our model is based on the trends of observed BLFs. We introduce the merging time-scale effect to explain the variation of BLFs, which has not dealt with any physical process of galaxy pairs. However, more realistic modeling of the d_p distribution involves a variety of complex factors, e.g., the birth rate of the galaxy pairs in the hierarchical structure, and the specific orbital parameters of pair members, which are beyond the scope of this study. Although our model is very simple and has many uncertainties, it *indeed can distinguish* different merging time-scale models. None of the models, in which the merging time-scale only dependent on the mass ratio of pair members, could reproduce the trends of observed BLFs. To our knowledge, our simple modeling *might be* the first time that the merging time-scale of galaxy pairs could be constrained by observational data.

Switches our attention to the brightening of galaxies from enhanced star formation modeled in Section 4.3, the parameterization of ΔM_r with Equation 24 is also quite simplified. First, during the parameterization of the ‘original’ star formation activity of galaxies, we have

taken the typical sSFR value of the widest galaxy pairs ($1.45 \times 10^{-10} \text{yr}^{-1}$) for all star-forming galaxies. Nevertheless, the sSFR of the star-forming galaxies in the local universe is not constant. A fitting of the main sequence of SDSS galaxies shows that $\log(\text{SFR}/M_\star) = -0.35(\log M_\star - 10) - 9.83$ (Salim et al. 2007). Therefore, a simple constant sSFR assumption might under/over estimate the brightening magnitude for low/high mass galaxies (see Equation 24). However, as shown by Equation 24, the effect on ΔM_r from the variation of sSFR could be partly compensated by the effect of its byproducts on Υ_0 . The galaxies with larger sSFR values also have averagely bluer colors and lower mass-to-light ratios. Combining these two effects, we have estimated that a factor of two times higher or lower sSFR brings a difference of brightening magnitude ~ 0.02 mag. Second, we have used only two global parameters, SFR enhancement strength f_Δ and duration time τ , to figure out the brightening process and omit their variation among different configurations of galaxy pairs. Many observations have shown that the SFR is more significantly enhanced in major merger pairs than minor merger pairs (Ellison et al. 2008; Davies et al. 2015). However, for the minor merger pairs, despite lower f_Δ , they also would have larger τ values (Cox et al. 2008; Davies et al. 2016). Combining these effects together, the average brightening magnitude of galaxies in pairs with different configurations may still be well approximated as a constant. Finally, it is worth mentioning that we have not taken the enhanced emissions from H II regions and nuclear activities into account. For the newborn stars, the H II regions only contribute $\sim 4\%$ of r -band flux (through H α and [N II] emission lines, Mármol-Queraltó et al. 2016). For the nuclear activities, the fraction of optical AGNs is shown to be dependent on the galaxy pair environment very weakly (Argudo-Fernández et al. 2016). Despite all the uncertainties listed above and other subtle effects which we have not discussed (e.g., the fraction of star-forming galaxies in pairs), our statistical approach, which takes characteristic values of f_Δ and τ to represent the overall/average brightening of all galaxy pairs, is still quite instructive.

In summary, the two toy models presented in this section have successfully characterized the general variation of the BLF of galaxy pairs, which bring new ideas on the study of both the galaxy merging time-scale and the star formation enhancement during the close-pair phase. To further accomplish this study, a full and detailed picture of the galaxy pair evolution is required, which could be gradually manifested through the combinations of the large sample statistics (e.g. this study),

the state-of-art numerical simulations(e.g. cosmological simulation with baryon physics, [Rodriguez-Gomez et al. 2015](#); [Sparre & Springel 2016](#)), and the detailed observations of the galaxy pairs in different merging phases (e.g. integral-field-spectroscopy study, [Yuan et al. 2018](#); [Fu et al. 2018](#)).

5. SUMMARY

In this study, we have compiled a sample of 46,510 isolated galaxy pairs based on the SDSS Main Galaxy Sample. We also benefit from a significant number of extra redshifts from other surveys(e.g., the LAMOST spectral and GAMA surveys). The completeness of $\theta \leq 55''$ pairs in our sample is significantly improved compared to previous SDSS-based galaxy pair samples.

Based on our large galaxy pair sample, we have calculated the BLF of galaxy pairs and studied its dependence on the projected distance between pair members d_p in detail. We find that the BLF degenerates into the LF of single galaxies at large distance ($d_p \geq 150 h^{-1}$ kpc), which indicates that galaxy-galaxy interaction starts from $d_p \leq 150 h^{-1}$ kpc. At $50 h^{-1}$ kpc $\leq d_p \leq 150 h^{-1}$ kpc, the BLFs deviate from the LFs of single galaxies significantly, where both the total magnitude of galaxy pairs and magnitude gap between pair members increase as d_p decrease. By integrating the BLFs of galaxy pairs, we also have obtained the ULF of galaxy pairs. Comparing with BLFs, the ULFs only show weak dependence on d_p .

The BLF variation is consistent with a physical scenario where the dynamic friction leads to massive and major merger pairs more rapidly merging. For the closest galaxy pairs ($10 h^{-1}$ kpc $\leq d_p \leq 50 h^{-1}$ kpc), the average magnitude of pair members shows an overall brightening trend, which manifests the enhanced star formation in this close-pair phase. It might be the first time that our statistical study reveals observational evidence for the merging time-scale of galaxy pairs. Our conclusion on the merging time-scale approximation, $T_m \propto (L_1/L_2)^{0.4}(L_1+L_2)^{-0.33}$, qualitatively agrees with

the conclusion from dark matter only numerical simulations of [Jiang et al. \(2014\)](#). From the overall brightening of $\Delta M_r \approx 0.04$ mag for the close pairs, we conclude that the starburst time-scale is about 0.4 Gyr considering 40% sSFR enhancement, which strengthens the conclusions from other observational studies(e.g. [Woods et al. 2010](#)) and numerical simulations(e.g. [Cox et al. 2008](#)).

In this study, we have only calculated the BLFs of galaxy pairs in the SDSS r -band. In principle, such measurements can be applied to other SDSS bands. Combining the BLFs in multi-bands will provide further constraints and insights on the galaxy-galaxy interaction in galaxy pairs. With the on-going data release of LAMOST spectral survey, the completeness of the galaxy pair sample can be further improved. Then, we expect a future study of the BLFs of galaxy pairs in other SDSS bands and for other detailed sub-samples(e.g., different morphology configurations).

This work is supported by the National Natural Science Foundation of China (No. 11573050 and 11433003) and the Science Foundation of Shanghai (No. 16ZR1442100). The authors thank Hugh Jones for carefully reading the manuscript and useful suggestions.

This work has made use of data products from the Sloan Digital Sky Survey (SDSS, <http://www.sdss.org>), the Large Sky Area Multi-Object Fibre Spectroscopic Telescope (LAMOST, <http://www.lamost.org>), the GAMA survey(<http://www.gama-survey.org>). Thanks for their tremendous efforts on the surveying work.

Guoshoujing Telescope (the Large Sky Area Multi-Object Fiber Spectroscopic Telescope LAMOST) is a National Major Scientific Project built by the Chinese Academy of Sciences. Funding for the project has been provided by the National Development and Reform Commission. LAMOST is operated and managed by the National Astronomical Observatories, Chinese Academy of Sciences.

REFERENCES

- Abazajian, K. N., Adelman-McCarthy, J. K., Agüeros, M. A., et al. 2009, *ApJS*, 182, 543, doi: [10.1088/0067-0049/182/2/543](https://doi.org/10.1088/0067-0049/182/2/543)
- Abolfathi, B., Aguado, D. S., Aguilar, G., et al. 2018, *ApJS*, 235, 42, doi: [10.3847/1538-4365/aa9e8a](https://doi.org/10.3847/1538-4365/aa9e8a)
- Alpaslan, M., Driver, S., Robotham, A. S. G., et al. 2015, *MNRAS*, 451, 3249, doi: [10.1093/mnras/stv1176](https://doi.org/10.1093/mnras/stv1176)
- Argudo-Fernández, M., Shen, S., Sabater, J., et al. 2016, *A&A*, 592, A30, doi: [10.1051/0004-6361/201628232](https://doi.org/10.1051/0004-6361/201628232)
- Baldry, I. K., Robotham, A. S. G., Hill, D. T., et al. 2010, *MNRAS*, 404, 86, doi: [10.1111/j.1365-2966.2010.16282.x](https://doi.org/10.1111/j.1365-2966.2010.16282.x)
- Ball, N. M., Loveday, J., Brunner, R. J., Baldry, I. K., & Brinkmann, J. 2006, *MNRAS*, 373, 845, doi: [10.1111/j.1365-2966.2006.11082.x](https://doi.org/10.1111/j.1365-2966.2006.11082.x)
- Barton, E. J., Geller, M. J., & Kenyon, S. J. 2000, *ApJ*, 530, 660, doi: [10.1086/308392](https://doi.org/10.1086/308392)
- Bell, E. F., McIntosh, D. H., Katz, N., & Weinberg, M. D. 2003, *ApJS*, 149, 289, doi: [10.1086/378847](https://doi.org/10.1086/378847)

- Blanton, M. R., & Roweis, S. 2007, *AJ*, 133, 734, doi: [10.1086/510127](https://doi.org/10.1086/510127)
- Blanton, M. R., Hogg, D. W., Bahcall, N. A., et al. 2003a, *ApJ*, 592, 819, doi: [10.1086/375776](https://doi.org/10.1086/375776)
- . 2003b, *ApJ*, 594, 186, doi: [10.1086/375528](https://doi.org/10.1086/375528)
- Blanton, M. R., Schlegel, D. J., Strauss, M. A., et al. 2005, *AJ*, 129, 2562, doi: [10.1086/429803](https://doi.org/10.1086/429803)
- Boylan-Kolchin, M., Ma, C.-P., & Quataert, E. 2008, *MNRAS*, 383, 93, doi: [10.1111/j.1365-2966.2007.12530.x](https://doi.org/10.1111/j.1365-2966.2007.12530.x)
- Bruzual, G., & Charlot, S. 2003, *MNRAS*, 344, 1000, doi: [10.1046/j.1365-8711.2003.06897.x](https://doi.org/10.1046/j.1365-8711.2003.06897.x)
- Colpi, M. 1998, *ApJ*, 502, 167, doi: [10.1086/305878](https://doi.org/10.1086/305878)
- Colpi, M., Mayer, L., & Governato, F. 1999, *ApJ*, 525, 720, doi: [10.1086/307952](https://doi.org/10.1086/307952)
- Cox, T. J., Jonsson, P., Somerville, R. S., Primack, J. R., & Dekel, A. 2008, *MNRAS*, 384, 386, doi: [10.1111/j.1365-2966.2007.12730.x](https://doi.org/10.1111/j.1365-2966.2007.12730.x)
- Cui, X.-Q., Zhao, Y.-H., Chu, Y.-Q., et al. 2012, *Research in Astronomy and Astrophysics*, 12, 1197, doi: [10.1088/1674-4527/12/9/003](https://doi.org/10.1088/1674-4527/12/9/003)
- Davies, L. J. M., Robotham, A. S. G., Driver, S. P., et al. 2015, *MNRAS*, 452, 616, doi: [10.1093/mnras/stv1241](https://doi.org/10.1093/mnras/stv1241)
- Davies, L. J. M., Robotham, A. S. G., Driver, S. P., et al. 2016, *MNRAS*, 455, 4013, doi: [10.1093/mnras/stv2573](https://doi.org/10.1093/mnras/stv2573)
- Domingue, D. L., Xu, C. K., Jarrett, T. H., & Cheng, Y. 2009, *ApJ*, 695, 1559, doi: [10.1088/0004-637X/695/2/1559](https://doi.org/10.1088/0004-637X/695/2/1559)
- Efstathiou, G., Ellis, R. S., & Peterson, B. A. 1988, *MNRAS*, 232, 431, doi: [10.1093/mnras/232.2.431](https://doi.org/10.1093/mnras/232.2.431)
- Ellison, S. L., Patton, D. R., Mendel, J. T., & Scudder, J. M. 2011, *MNRAS*, 418, 2043, doi: [10.1111/j.1365-2966.2011.19624.x](https://doi.org/10.1111/j.1365-2966.2011.19624.x)
- Ellison, S. L., Patton, D. R., Simard, L., & McConnachie, A. W. 2008, *AJ*, 135, 1877, doi: [10.1088/0004-6256/135/5/1877](https://doi.org/10.1088/0004-6256/135/5/1877)
- Fu, H., Steffen, J. L., Gross, A. C., et al. 2018, *ApJ*, 856, 93, doi: [10.3847/1538-4357/aab364](https://doi.org/10.3847/1538-4357/aab364)
- Guo, H., Zehavi, I., & Zheng, Z. 2012, *ApJ*, 756, 127, doi: [10.1088/0004-637X/756/2/127](https://doi.org/10.1088/0004-637X/756/2/127)
- Hernández-Toledo, H. M., Avila-Reese, V., Conselice, C. J., & Puerari, I. 2005, *AJ*, 129, 682, doi: [10.1086/427134](https://doi.org/10.1086/427134)
- Hernández-Toledo, H. M., Avila-Reese, V., Salazar-Contreras, J. R., & Conselice, C. J. 2006, *AJ*, 132, 71, doi: [10.1086/504157](https://doi.org/10.1086/504157)
- Jiang, C. Y., Jing, Y. P., Faltenbacher, A., Lin, W. P., & Li, C. 2008, *ApJ*, 675, 1095, doi: [10.1086/526412](https://doi.org/10.1086/526412)
- Jiang, C. Y., Jing, Y. P., & Han, J. 2014, *ApJ*, 790, 7, doi: [10.1088/0004-637X/790/1/7](https://doi.org/10.1088/0004-637X/790/1/7)
- Kewley, L. J., Rupke, D., Zahid, H. J., Geller, M. J., & Barton, E. J. 2010, *ApJL*, 721, L48, doi: [10.1088/2041-8205/721/1/L48](https://doi.org/10.1088/2041-8205/721/1/L48)
- Lacey, C., & Cole, S. 1994, *MNRAS*, 271, 676, doi: [10.1093/mnras/271.3.676](https://doi.org/10.1093/mnras/271.3.676)
- Lambas, D. G., Tissera, P. B., Alonso, M. S., & Coldwell, G. 2003, *MNRAS*, 346, 1189, doi: [10.1111/j.1365-2966.2003.07179.x](https://doi.org/10.1111/j.1365-2966.2003.07179.x)
- Liske, J., Baldry, I. K., Driver, S. P., et al. 2015, *MNRAS*, 452, 2087, doi: [10.1093/mnras/stv1436](https://doi.org/10.1093/mnras/stv1436)
- Liu, X., Shen, Y., Strauss, M. A., & Hao, L. 2011, *ApJ*, 737, 101, doi: [10.1088/0004-637X/737/2/101](https://doi.org/10.1088/0004-637X/737/2/101)
- Lotz, J. M., Jonsson, P., Cox, T. J., & Primack, J. R. 2010a, *MNRAS*, 404, 575, doi: [10.1111/j.1365-2966.2010.16268.x](https://doi.org/10.1111/j.1365-2966.2010.16268.x)
- . 2010b, *MNRAS*, 404, 590, doi: [10.1111/j.1365-2966.2010.16269.x](https://doi.org/10.1111/j.1365-2966.2010.16269.x)
- Luo, A.-L., Zhao, Y.-H., Zhao, G., et al. 2015, *Research in Astronomy and Astrophysics*, 15, 1095, doi: [10.1088/1674-4527/15/8/002](https://doi.org/10.1088/1674-4527/15/8/002)
- Mandelbaum, R., Seljak, U., Kauffmann, G., Hirata, C. M., & Brinkmann, J. 2006, *MNRAS*, 368, 715, doi: [10.1111/j.1365-2966.2006.10156.x](https://doi.org/10.1111/j.1365-2966.2006.10156.x)
- Mármol-Queraltó, E., McLure, R. J., Cullen, F., et al. 2016, *MNRAS*, 460, 3587, doi: [10.1093/mnras/stw1212](https://doi.org/10.1093/mnras/stw1212)
- McNaught-Roberts, T., Norberg, P., Baugh, C., et al. 2014, *MNRAS*, 445, 2125, doi: [10.1093/mnras/stu1886](https://doi.org/10.1093/mnras/stu1886)
- Patton, D. R., Qamar, F. D., Ellison, S. L., et al. 2016, *MNRAS*, 461, 2589, doi: [10.1093/mnras/stw1494](https://doi.org/10.1093/mnras/stw1494)
- Patton, D. R., Torrey, P., Ellison, S. L., Mendel, J. T., & Scudder, J. M. 2013, *MNRAS*, 433, L59, doi: [10.1093/mnrasl/slt058](https://doi.org/10.1093/mnrasl/slt058)
- Robotham, A. S. G., Driver, S. P., Davies, L. J. M., et al. 2014, *MNRAS*, 444, 3986, doi: [10.1093/mnras/stu1604](https://doi.org/10.1093/mnras/stu1604)
- Rodriguez-Gomez, V., Genel, S., Vogelsberger, M., et al. 2015, *MNRAS*, 449, 49, doi: [10.1093/mnras/stv264](https://doi.org/10.1093/mnras/stv264)
- Salim, S., Boquien, M., & Lee, J. C. 2018, *ApJ*, 859, 11, doi: [10.3847/1538-4357/aabf3c](https://doi.org/10.3847/1538-4357/aabf3c)
- Salim, S., Rich, R. M., Charlot, S., et al. 2007, *ApJS*, 173, 267, doi: [10.1086/519218](https://doi.org/10.1086/519218)
- Salim, S., Lee, J. C., Janowiecki, S., et al. 2016, *ApJS*, 227, 2, doi: [10.3847/0067-0049/227/1/2](https://doi.org/10.3847/0067-0049/227/1/2)
- Schechter, P. 1976, *ApJ*, 203, 297, doi: [10.1086/154079](https://doi.org/10.1086/154079)
- Scudder, J. M., Ellison, S. L., Torrey, P., Patton, D. R., & Mendel, J. T. 2012, *MNRAS*, 426, 549, doi: [10.1111/j.1365-2966.2012.21749.x](https://doi.org/10.1111/j.1365-2966.2012.21749.x)
- Shen, S.-Y., Argudo-Fernández, M., Chen, L., et al. 2016, *Research in Astronomy and Astrophysics*, 16, 007, doi: [10.1088/1674-4527/16/3/043](https://doi.org/10.1088/1674-4527/16/3/043)

- Sodre, L., & Lahav, O. 1993, MNRAS, 260, 285,
doi: [10.1093/mnras/260.2.285](https://doi.org/10.1093/mnras/260.2.285)
- Sparre, M., & Springel, V. 2016, MNRAS, 462, 2418,
doi: [10.1093/mnras/stw1793](https://doi.org/10.1093/mnras/stw1793)
- Strauss, M. A., Weinberg, D. H., Lupton, R. H., et al. 2002, AJ, 124, 1810, doi: [10.1086/342343](https://doi.org/10.1086/342343)
- Takeuchi, T. T., Sakurai, A., Yuan, F.-T., Buat, V., & Burgarella, D. 2013, Earth, Planets, and Space, 65, 281,
doi: [10.5047/eps.2012.06.008](https://doi.org/10.5047/eps.2012.06.008)
- Tinker, J. L., Weinberg, D. H., Zheng, Z., & Zehavi, I. 2005, ApJ, 631, 41, doi: [10.1086/432084](https://doi.org/10.1086/432084)
- Toomre, A., & Toomre, J. 1972, ApJ, 178, 623,
doi: [10.1086/151823](https://doi.org/10.1086/151823)
- van den Bosch, F. C., Lewis, G. F., Lake, G., & Stadel, J. 1999, ApJ, 515, 50, doi: [10.1086/307023](https://doi.org/10.1086/307023)
- Velander, M., van Uitert, E., Hoekstra, H., et al. 2014, MNRAS, 437, 2111, doi: [10.1093/mnras/stt2013](https://doi.org/10.1093/mnras/stt2013)
- Woods, D. F., Geller, M. J., & Barton, E. J. 2006, AJ, 132, 197, doi: [10.1086/504834](https://doi.org/10.1086/504834)
- Woods, D. F., Geller, M. J., Kurtz, M. J., et al. 2010, AJ, 139, 1857, doi: [10.1088/0004-6256/139/5/1857](https://doi.org/10.1088/0004-6256/139/5/1857)
- Xu, C., & Sulentic, J. W. 1991, ApJ, 374, 407,
doi: [10.1086/170132](https://doi.org/10.1086/170132)
- Xu, C. K., Sun, Y. C., & He, X. T. 2004, ApJL, 603, L73,
doi: [10.1086/383223](https://doi.org/10.1086/383223)
- Yang, X., Mo, H. J., van den Bosch, F. C., et al. 2007, ApJ, 671, 153, doi: [10.1086/522027](https://doi.org/10.1086/522027)
- York, D. G., Adelman, J., Anderson, Jr., J. E., et al. 2000, AJ, 120, 1579, doi: [10.1086/301513](https://doi.org/10.1086/301513)
- Yuan, F.-T., Argudo-Fernández, M., Shen, S., et al. 2018, A&A, 613, A13, doi: [10.1051/0004-6361/201731865](https://doi.org/10.1051/0004-6361/201731865)
- Zhao, G., Zhao, Y.-H., Chu, Y.-Q., Jing, Y.-P., & Deng, L.-C. 2012, Research in Astronomy and Astrophysics, 12, 723, doi: [10.1088/1674-4527/12/7/002](https://doi.org/10.1088/1674-4527/12/7/002)